Multiple exchange in ^{3}He and in the Wigner solid

M. Roger

Institut Laue-Langevin, Boîte Postale 156X, F-38042 Grenoble (Cédex), France
and Service de Physique du Solide et de Résonance Magnétique, Direction de la Physique, Commissariat à l'Energie Atomique, Orme des Merisiers, Centre d'Etudes Nucléaires de Saclay, F-91191 Gif-sur-Yvette (Cédex), France*

(Received 6 February 1984; revised manuscript received 24 September 1984)

We use a multidimensional WKB calculation to determine the leading terms of a high-density series expansion for the multiple-exchange frequencies in solid ^{3}He. We also calculate, within the same formulation, the first terms of a low-density series expansion for exchange in the two-dimensional Wigner solid of electrons. The hierarchy between the exchange frequencies is dominated by the geometry of the lattice. Triple exchange is preponderant in the two-dimensional triangular lattice. This result holds for potentials as different as the $(\sigma/r)^{12}$ (solid ^{3}He) and the Coulomb potential (Wigner solid). Three-particle exchange also dominates in the hcp lattice. We find for a hypothetical high-density bcc ^{3}He solid the same hierarchy as that deduced from the experimental results at physical densities: The planar four-particle exchange K_P and the triple exchange J_t dominate, the folded four-particle exchange K_F is much lower. For both K_P and J_t the lengths of the exchange paths and the tunneling barrier heights are practically the same. We expect these results to be qualitatively valid at physical densities and understand why K_P and J_t depend similarly on the molar volume.

I. INTRODUCTION

It is now well established that three- and four-particle exchange processes play an essential role in hard-sphere quantum solids.[1] Most of the striking magnetic properties of bcc solid ^{3}He (phase diagram, high-temperature series expansions of the thermodynamical quantities, spin-wave spectrum, etc) have been interpreted with a multiple-exchange Hamiltonian including only planar cyclic four-spin exchange K_P and three-spin exchange J_t.[1] There is also evidence for multiple exchange in other quantum solids: For example, three-molecule exchange can explain the motional narrowing of the resonance line observed for HD impurities in hcp para-hydrogen.[2]

Calculation of the multiple-exchange frequencies from first principles is a large task. It requires an accurate evaluation of the wave function in low-probability regions. Simple approximations based on products of one-particle wave functions and Jastrow functions are unable to describe the behavior of the exact wave function in these low-probability regions.[1,3] Consequently, early calculations using these products[4,5] are irrelevant. Reasonable approximations of the wave function, taking the hard-core correlations correctly into account, have been proposed by Delrieu *et al.*[3,6] They lead to the conclusion that three-particle exchange dominates in triangular geometry (two-dimensional triangular lattice or three-dimensional hcp lattice), whereas, two-, three-, and four-particle exchange are of the same order of magnitude in the bcc solid. In bcc ^{3}He these approximations are, however, too rough to determine the hierarchy between the two kinds of four-particle—exchange cycles involving first neighbors: planar (K_P) and folded (K_F). (The experimental results can be explained only if $|K_P| > |K_F|$.)[1]

Exchange calculations become much easier if we restrict our ambition to the high-density limit. For ^{3}He at high density, the kinetic energy of the atoms (of the order of $\hbar^2/2ma^2$, a representing the interatomic spacing) becomes smaller than the potential energy [repulsive part of the Lennard-Jones potential, increasing as $(\sigma/a)^{12}$]. We can apply a multidimensional WKB (quasiclassical) approximation and determine, for each exchange frequency, the leading terms within a high-density series expansion in a/σ. We have published the main lines of this calculation in Ref. 7. The multidimensional WKB approximation was also used in a paper published at the same time by Avilov and Iordansky.[8]

The purpose of this paper is to present the details of this calculation and to apply it to various lattices. All kinds of two-, three-, and four-particle exchanges are investigated and compared for the two-dimensional triangular lattice and the three-dimensional hcp and bcc lattices (keeping in mind that for ^{3}He this approximation is more appropriate to the triangular and hcp lattice than to the bcc solid, which is not stable under high pressure). We also perform the same WKB approximation with other interacting potentials. In particular, we investigate two-, three-, and four-particle exchange in a two-dimensional Wigner solid of electrons.

For the Coulomb potential, the quasiclassical approximation applies at low densities when the kinetic energy, of the order of $\hbar^2/2ma^2$, becomes much smaller than the potential energy, decreasing in $1/a$; we determine the leading terms of a low-density series expansion in $1/a$. The following results are obtained: In a two-dimensional triangular lattice three-particle exchange dominates; the hierarchy between two- and three-particle exchange is the same with interactions as different as the $1/r$ and the $1/r^{12}$ potentials; it seems to be essentially determined by the geometry of the lattice. Three-particle exchange also

dominates in the hcp lattice.

In the bcc lattice with $1/r^{12}$ potential, the leading terms of our high-density series expansion give the following hierarchy: K_P (planar four-particle exchange) $> J_t$ (three-particle exchange) $> J_{\rm NN}$ (two-particle exchange) $> S_{IX}$ (six-particle exchange) $> K_F$ (folded four-particle exchange). (NN denotes nearest neighbor.) This calculation is the first which predicts a precise hierarchy between various exchange frequencies in bcc ^{3}He. This hierarchy is strikingly the same as that assumed in the phenomenological model which fits the data,[1] in particular, folded four-spin exchange appears to be negligible with respect to planar four-spin exchange.

As shown in the triangular lattice, the hierarchy between the exchange frequencies depends essentially on the lattice geometry and not on the precise shape of the potential. We expect that the results found in the high-density limit are still valid at larger molar volumes where the kinetic-energy effects can be included to some extent in an effective potential (see Sec. V). For the dominant exchanges, K_P, J_t, and $J_{\rm NN}$ the lengths of the exchange paths are practically equal and the heights of the potential barriers comparable; we expect this result to be still approximately valid at lower densities and understand the reason why, according to the experimental data, J_t and K_P must vary according to similar laws in terms of the density.[9–12] We thus remove the last objections raised against the multiple-exchange model.

This paper is presented according to the following scheme: The main hypotheses which led to the concept of a multiple-exchange Hamiltonian are recalled in Sec. II. The calculation of the exchange frequencies is presented in Sec. III using the imaginary-time version of the Feynman path-integral formalism. The multidimensional WKB series expansion is derived in Sec. IV, and is applied to the two-dimensional triangular lattice with various potentials [$(\sigma/r)^{12}$, full Lennard-Jones potential, Coulomb potential] and to the three-dimensional hcp and bcc lattices.

In Sec. V we discuss the extrapolation of our calculation to ^{3}He at physical densities, briefly review earlier (crude) approximations which have been proposed for the low densities of the bcc phase, and discuss the variations of the exchange parameters with the molar volume.

II. GENERALITIES ON THE MULTIPLE-EXCHANGE HAMILTONIAN

In ^{3}He the Hamiltonian does not depend explicitly on the spins, and hence the Schrödinger equation only determines the orbital part of the wave function. The spin dependence appears by writing the antisymmetry condition for the total wave function.

Since the Hamiltonian is invariant by any permutation of the coordinates, its eigenvalues and eigenvectors are classified according to the irreducible representations of the permutation group. Each of these representations can be associated with a Young diagram.[13] The total antisymmetric wave function ψ^T can be written as a bilinear product of orbital wave functions $\psi_\mu^{(r)}$ and spin-wave functions $\xi_\nu^{(\sigma)}$,

$$\psi^T=\sum_{\mu,\nu} C_{\mu\nu}\psi_\mu^{(r)}\xi_\nu^{(\sigma)} . \tag{2.1}$$

The $\psi_\mu^{(r)}$ have the symmetry corresponding to a given representation of the permutation group (associated with a given Young diagram) and the $\xi_\nu^{(\sigma)}$ belong to the representation associated with the complementary Young diagram (obtained by exchanging the lines and columns).

The energy levels can be determined by first considering the orbital part of the wave function and solving the Schrödinger equation in the $3N$-dimensional space representing the coordinates of N distinguishable particles. We take a localized picture of the solid. The atoms spend most of the time at positions around the lattice sites and exchange occurs rarely (in bcc ^{3}He the exchange frequency is 10^{-4} smaller than the Debye frequency). Following Thouless,[14] we call the regions of the $3N$-dimensional configuration space corresponding to the highest probability for the wave function "cavities" (each particle is around a given lattice site).

There are $N!$ cavities Ω_P corresponding to the $N!$ permutations P of N distinguishable particles on N labeled sites. If there were no exchange, each cavity would be isolated and the ground state would be $N!$ times degenerate.

If the exchange effects are small, but finite, the degenerate ground state splits into a band which can be reasonably described by a hopping Hamiltonian between isolated pairs of cavities,

$$\mathscr{H}_{\rm ex}=-\sum_P J_P P^{(r)} . \tag{2.2}$$

$P^{(r)}$ represents the permutation operator acting on the coordinates. J_P corresponds to the energy splitting for tunneling between two *isolated* cavities Ω_I and Ω_P. The summation is extended to the $N!$ permutations P of N particles.

From relation (2.1) and related remarks, $\mathscr{H}_{\rm ex}$ [relation (2.2)] can be expressed as well in terms of the permutation operators $P^{(\sigma)}$ acting on the spin variables,

$$\mathscr{H}_{\rm ex}=-\sum_P (-1)^p J_P P^{(\sigma)} . \tag{2.3}$$

The factor $(-1)^p$ (p, parity of the permutation) comes from the relation

$$P\psi^T=P^{(r)}P^{(\sigma)}\psi^T=(-1)^p\psi^T .$$

(For more details about the derivation of the exchange Hamiltonian, see Refs. 1 and 14.)

As first shown by Thouless,[14] even and odd permutations lead respectively, to ferromagnetism and antiferromagnetism. Consequently, all constants J_P in relation (2.3) have the same *positive* sign. Note that here we take the opposite-sign convention of that of Ref. 1, in the definition of the J_P's. We adopt this choice because it will be more convenient in the following to deal with positive frequencies.

III. CALCULATION OF THE EXCHANGE FREQUENCIES

In this section we choose an approach based on the imaginary-time version of the Feynman path-integral

method.[15] We suggest a simple scheme to compare the exchange frequencies, using a Monte Carlo integration (this is certainly the most efficient method for future exchange calculations at low densities). The quasiclassical approximation is then derived from this approach in a straightforward way.

A. Exchange via path-integral methods

The probability amplitude for going from the initial configuration X_I at time $-t/2$ to the final position X_P at time $t/2$ is expressed as (see Ref. 15)

$$\langle X_P \mid e^{-i(Ht/\hbar)} \mid X_I \rangle = C \int [dX] e^{iS_0/\hbar} , \tag{3.1}$$

where H is the Hamiltonian, S_0 is the action

$$S_0 = \int_{-t/2}^{t/2} d\tau \left[\frac{m}{2} \left(\frac{dX}{d\tau} \right)^2 - V[X(\tau)] \right] , \tag{3.2}$$

and $[dX]$ means the integration over all paths $X(\tau)$ obeying the boundary condition

$$X(\tau = -t/2) = X_I , \quad X(\tau = +t/2) = X_P .$$

C is a normalization constant.

For our exchange problem, X_I and X_P represent, respectively, the centers of the two cavities Ω_I and Ω_P.

X_I: $3N$-particle configuration, a particle number i being at site $\vec{R}_i$,

$$\vec{r}_1 = \vec{R}_1 ,$$
$$\vec{r}_2 = \vec{R}_2 ,$$
$$\dots ,$$
$$\vec{r}_\nu = \vec{R}_\nu ,$$
$$\dots ,$$
$$\vec{r}_N = \vec{R}_N .$$

X_P: configuration deduced from X_I by the permutation P of ν particles,

$$\vec{r}_1 = \vec{R}_{n_1} ,$$
$$\vec{r}_2 = \vec{R}_{n_2} ,$$
$$\dots ,$$
$$\vec{r}_\nu = \vec{R}_{n_\nu} ,$$
$$\vec{r}_{\nu+1} = \vec{R}_{\nu+1} ,$$
$$\dots ,$$
$$\vec{r}_N = \vec{R}_N .$$

[where $n_j = P(j)$].

The parametrization of the paths $X(\tau)$ by an imaginary time ($\tau = -i\theta$) leads to the imaginary-time version of the path-integral equations,

$$\langle X_P \mid e^{-HT/\hbar} \mid X_I \rangle = C \int [dX] e^{-S/\hbar} . \tag{3.1'}$$

S is the Euclidean action,

$$S = \int_{-T/2}^{T/2} d\theta \left[\frac{m}{2} \left(\frac{dX}{d\theta} \right)^2 + V[X(\theta)] \right] , \tag{3.2'}$$

and T plays the role of an inverse temperature.

If $\{E_n, \mid \psi_n \rangle\}$ represents a complete set of eigenstates of the Hamiltonian, the left-hand side of (3.1') can be expanded,

$$\langle X_P \mid e^{-HT/\hbar} \mid X_I \rangle = \sum_n e^{-E_n T/\hbar} \langle X_P \mid \psi_n \rangle \langle \psi_n \mid X_I \rangle . \tag{3.3}$$

At large T, $T \gg \hbar/E_0$ (E_0 is the ground-state energy), the leading terms in (3.3) come from the lowest-energy modes of the two coupled cavities Ω_I and Ω_P: $\mid \psi^S \rangle$ with energy $E^S = E_0 - J_P$ and $\mid \psi^A \rangle$ with energy $E^A = E_0 + J_P$.

In the small exchange limit the amplitudes of the wave functions $\mid \psi^S \rangle$ and $\mid \psi^A \rangle$ at the cavity centers are practically the same and are equal to the amplitude φ_0 of the wave function for two isolated cavities,

$$\langle \psi^S \mid X_I \rangle = \langle \psi^S \mid X_P \rangle \simeq \langle \psi^A \mid X_I \rangle = -\langle \psi^A \mid X_P \rangle = \varphi_0 .$$

With these conditions, relation (3.3) leads to

$$\langle X_P \mid e^{-HT/\hbar} \mid X_I \rangle = 2\varphi_0^2 e^{-E_0 T/\hbar} \sinh \left[\frac{JT}{\hbar} \right] . \tag{3.4}$$

If we choose T such that

$$\hbar/E_0 \ll T \ll \hbar/J_P , \tag{3.5}$$

we obtain, from (3.1)–(3.5),

$$J_P = \frac{\hbar C e^{E_0 T/\hbar}}{2T\varphi_0^2} \int [dX] e^{-S/\hbar} . \tag{3.6}$$

We first need an accurate determination of the ground-state energy E_0 and of the wave function φ_0 for two isolated cavities in order to apply (3.6).

However, the ratio between two exchange frequencies could be more easily evaluated in the following way. Let us consider Ω_I and two permuted cavities: Ω_P corresponding to the permutation P of ν particles and $\Omega_{P'}$ corresponding to another permutation P' of ν' particles. The factors φ_0^2 and $e^{E_0 T/\hbar}$ cancel if we evaluate directly the ratio between the corresponding exchange frequencies J_P and $J_{P'}$,

$$J_P / J_{P'} = \int [dX]_P e^{-S/\hbar} \Big/ \int [dX]_{P'} e^{-S/\hbar} , \tag{3.7}$$

where $[dX]_P$ and $[dX]_{P'}$ denote the integration over the paths starting from the center of Ω_I at $\theta = -T/2$ and ending, respectively, at the center of Ω_P and the center of $\Omega_{P'}$ at $\theta = +T/2$ [remember that T must obey the condition (3.5)]. The path integrals in (3.7) could be performed by the usual Monte Carlo techniques.[16] We suggest this scheme as a good starting point for future exact calculations of the exchange frequencies at all densities. It is interesting to investigate first the hierarchy between various multiple-exchange frequencies in the simple quasiclassical limit.

B. Quasiclassical limit

If $\hbar^2/m$, is small, the integrals in (3.6) and (3.7) are dominated by the path along which the action S is stationary, $\delta S=0$. The condition $\delta S=0$ applied to (3.2') leads to

$$\frac{m d^2 X_{\rm cl}}{d\theta^2}=\vec{\nabla} V(X_{\rm cl}) \tag{3.8}$$

($\vec{\nabla}$ represents the gradient), which is the equation for the classical trajectory $X_{\rm cl}(\theta)$ of a particle moving under a potential $-V$ (the origin of the sign inversion comes from the parametrization with imaginary time).

Through the integration of (3.8) we obtain

$$\tfrac{1}{2}m\left[\frac{dX_{\rm cl}}{d\theta}\right]^2-V(X_{\rm cl})=\text{const}=-E_0 . \tag{3.9}$$

This relation defines the energy E_0. Using (3.2') and (3.9), the classical action can be expressed as

$$S(X_{\rm cl})=\int_{-T/2}^{T/2} d\theta\left[m\left[\frac{dX_{\rm cl}}{d\theta}\right]^2+E_0\right]$$

$$=E_0 T+\int_{X_I}^{X_P} dx[2m(V-E_0)]^{1/2} ,$$

where dx denotes the arc length along the line $X_{\rm cl}$. From (3.6) we obtain the leading terms for the exchange,

$$J_P\sim\exp\left[-\frac{1}{\hbar}\int_{X_I}^{X_P} dx[2m(V-E_0)]^{1/2}\right], \tag{3.10}$$

where the integral is taken over the classical path for a particle moving from X_I to X_P with energy $-E_0$ under a potential $-V$. In the literature, this exchange path has been called the "most probable escape path" (MPEP).[17,18]

IV. EXCHANGE IN THE QUASICLASSICAL LIMIT FOR VARIOUS LATTICES AND INTERACTING POTENTIALS

In this section we investigate the quasiclassical limit for various lattices and interacting potentials. In solid ^{3}He we determine the first terms of a high-density series expansion in σ/a for the two-dimensional triangular lattice and for the hcp and bcc lattice with interacting potential $V=4\epsilon(\sigma/r)^{12}$ (repulsive part of the Lennard-Jones potential). For the heavier rare gases we keep the full Lennard-Jones potential

$$V=4\epsilon[(\sigma/r)^{12}-(\sigma/r)^6]$$

and perform the expansion in $\hbar/\sqrt{m}$. We also consider the two-dimensional Wigner solid of electrons with $1/r$ Coulomb potential and calculate the first terms of a low-density series expansion.

A. Formulations

The quasiclassical limit has been derived in the preceding section from path integrals. However, for the reader who is more familiar with the WKB formalism we shall describe here this strictly equivalent approach.[19]

1. *With the Lennard-Jones pair-interaction potential*

a. Expression of the wave function. In reduced units, $\vec{\rho}=(\vec{r}_1/a,\vec{r}_2/a,\ldots,\vec{r}_N/a)$ (a is the distance between first neighbors), the Schrödinger equation is written as

$$-\frac{\hbar^2}{2ma^2}\Delta\psi(\vec{\rho})+4\epsilon\sum_{\substack{i,j=1\\ i<j}}^{N}\left[\left[\frac{\sigma}{a}\right]^{12}|\vec{\rho}_{ij}|^{-12}-\left[\frac{\sigma}{a}\right]^{6}|\vec{\rho}_{ij}|^{-6}\right]\psi(\vec{\rho})$$

$$=E\psi(\vec{\rho}) . \tag{4.1}$$

We take the usual 12-6 Lennard-Jones pair-interaction potential ($\epsilon=-10.22$ K and $\sigma=2.556$ Å for ^{3}He). The quasiclassical calculation is valid when the ratio of the kinetic energy to the potential energy is small. For rare gases heavier than ^{3}He we keep the full 12-6 Lennard-Jones potential and choose the ratio $\hbar/\sqrt{m}$ as the small parameter for the WKB series expansion.

In solid ^{3}He, the quasiclassical limit is considered at very high densities when the leading term (repulsive part) of the Lennard-Jones potential, increasing as $(\sigma/a)^{12}$, becomes larger than the kinetic-energy term in $\hbar^2/a^2$. The appropriate parameter for the WKB series expansion is the square root of the ratio of the kinetic energy to the repulsive part of the Lennard-Jones potential,

$$g=\frac{\hbar}{(8m\sigma^2\epsilon)^{1/2}}\left[\frac{a}{\sigma}\right]^5 . \tag{4.2}$$

In the WKB formalism, the wave function is written as

$$\psi(\vec{\rho})=A\exp\left[\frac{i}{g}W(\vec{\rho})\right] . \tag{4.3}$$

We assume that $W(\vec{\rho})$ can be expanded in a power series of a/σ or $\alpha=g^{1/5}$,

$$W(\vec{\rho})=W_0+\alpha W_1(\vec{\rho})+\cdots+\alpha^n W_n(\vec{\rho}) , \tag{4.4}$$

with $W_i(\vec{\rho})$ independent of a.

We substitute (4.4) and (4.3) into the Schrödinger equation (4.1).

(i) At lowest order in g, we obtain

$$[\vec{\nabla} W_0(\vec{\rho})]^2+[V^{12}(\vec{\rho})-E_0]=0 . \tag{4.5}$$

$V^{12}(\vec{\rho})$ is the repulsive part of the Lennard-Jones potential,

$$V^{12}(\vec{\rho})=\sum_{\substack{i,j=1\\ i<j}}^{N}|\vec{\rho}_{ij}|^{-12} .$$

Exchange corresponds to classically forbidden regions with $V^{12}>E_0$, and W_0 is purely imaginary. The quantity $W_0^*=-iW_0$ obeys the Hamilton-Jacobi equation for a classical particle moving under a potential $-V^{12}$ with energy $-E_0$; hence,

$$W_0^*(\vec{\rho})=\int_{\vec{\rho}_0}^{\vec{\rho}}[V^{12}(\vec{\rho}(\theta))-E_0]^{1/2}d\theta , \tag{4.6}$$

where the integral is taken along the classical trajectory $\mathscr{L}(\theta)$ which makes the action W_0^* stationary and θ is chosen as the arc length along the line $\mathscr{L}$.

(ii) The next orders in α are W_5 and W_6: the substitution of (4.3) and (4.4) into (4.1) leads to $W_1=W_2=W_3=W_4=0$ and

$$-i\Delta W_0(\vec{\rho})+2\vec{\nabla}W_5(\vec{\rho})\cdot\vec{\nabla}W_0(\vec{\rho})=E_5 , \tag{4.7}$$

$$2\vec{\nabla}W_0(\vec{\rho})\cdot\vec{\nabla}W_6(\vec{\rho})-\left[\frac{8\epsilon m\sigma^2}{\hbar^2}\right]^{3/5}\sum_{\substack{i,j=1\\ i<j}}^{N}|\vec{\rho}_{ij}^{-6}|=E_6 . \tag{4.8}$$

W_5 leads in the phase factor of ψ [relation (4.3)] to a term independent of g. The term W_6 coming directly from the attractive part of the Lennard-Jones potential leads to a term in α or $g^{1/5}$ in the phase of ψ.

b. Exchange frequency. In terms of the wave functions, the exchange frequency J_P is expressed as a flux integral[1,4]

$$J_P=\frac{E^A-E^S}{2}=\frac{\hbar^2}{4m}\frac{\int_\Sigma[\psi^A(\vec{\nabla}\psi^S)-\psi^S(\vec{\nabla}\psi^A)]d\vec{S}}{\int_v|\psi^S\psi^A|dv} \tag{4.9}$$

through the $(3N-1)$-dimensional median hyperplane Σ equidistant from the configurations X_I and X_P. v is the half-space limited by Σ; ψ^S and ψ^A represent, respectively, the even and odd modes of the two coupled cavities Ω_I and Ω_P.

The flux integral (4.9) can be rewritten in terms of the function $\psi_1=\frac{1}{2}(\psi^S+\psi^A)$ localized in the cavity Ω_I and the function $\psi_2=\frac{1}{2}(\psi^S-\psi^A)$ obtained from ψ_1 by reflection with respect to the median hyperplane Σ,

$$J_P\simeq\frac{\hbar^2}{2m}\frac{\int_\Sigma[\psi_1(\vec{\nabla}\psi_2)-(\psi_2)(\vec{\nabla}\psi_1)]d\vec{S}}{\int_v\psi_1^2dv} . \tag{4.10}$$

We take into account that around the center of Ω_I, $\psi_1\simeq\psi^S\sim\psi^A$, and hence

$$\int_v\psi_S\psi_A dv\simeq\int_v\psi_1^2dv .$$

Note that in relation (4.10) the functions ψ_1 and ψ_2 do not need to be normalized.

(i) Lowest order in g: We consider the classical path (MPEP) $\mathscr{L}(\theta)$ joining the centers of the two cavities Ω_I and Ω_P. In the exchange configurations $(V-E>0)$ the wave function is maximum along $\mathscr{L}(\theta)$ and decreases exponentially in the directions perpendicular to the path. As done in Refs. 17 and 18 it is convenient to introduce a curvilinear coordinate system related to the MPEP. At each point M of the path we define the local coordinate system by the unit vector $\vec{\theta}$ along the tangent to $\mathscr{L}(\theta)$ and $3N-1$ orthogonal unit vectors $\vec{n}_i$ in the subspace orthogonal to $\vec{\theta}$. We expand $V-E_0$ and W^* in a power series of the coordinates η_i in the $(3N-1)$-dimensional subspace orthogonal to $\vec{\theta}$.[17] We write

$$V^{12}-E_0=V_0(\theta)+\sum_i\eta_iV_1^i(\theta)+\tfrac{1}{2}\sum_{i,j}\eta_i\eta_jV_2^{ij}(\theta)+\cdots , \tag{4.11a}$$

$$W^*=W_0^*(\theta)+\tfrac{1}{2}\sum_{i,j}\eta_i\eta_jW_2^{ij}(\theta)+\cdots . \tag{4.11b}$$

(The linear term in W^* vanishes[17] because the classical path corresponds to a minimum of the action.)

The relations between the W_2^{ij} and V_1^i, V_2^{ij} are obtained by inserting (4.11b) into (4.3) and substituting the result into the Schrödinger equation (4.1).

At zeroth order in η_i we again obtain the equation (4.6),

$$W_0^*(\theta)=\int^\theta(V_0)^{1/2}(s)ds .$$

At first and second order with respect to the η_i's, the full equations taking into account the curvature of the path are intricate (cf. Ref. 17). As a rough approximation we will assume that the curvature of the path can be neglected in the neighborhood of the median hyperplane Σ. In this case we obtain

$$\left[\frac{d}{d\theta}W_0^*\right]\frac{d}{d\theta}W_2^{ij}+\sum_k W_2^{ik}W_2^{kj}\simeq\tfrac{1}{2}V_2^{ij} .$$

The coordinate system $(\vec{\theta},\vec{n}_i)$ can always be chosen such that the tensor V_2^{ij} is diagonal; in this case the preceding equation leads to

$$W_2^{ij}=0 \quad \text{for } i\neq j ,$$

$$\left[\frac{d}{d\theta}W_0^*\right]\frac{d}{d\theta}W_2^{ij}+(W_2^{ii})^2\simeq\tfrac{1}{2}V_2^{ii} .$$

At the middle of the path, $\theta=L$ (intersection X_M of the path with the median hyperplane Σ), $(d/d\theta)W_0$ cancels; hence W_2^{ii} is simply equal to the square root of $V_2^{ii}/2$,

$$W_2^{ii}\simeq(V_2^{ii})^{1/2}/\sqrt{2} . \tag{4.12}$$

Inserting (4.12) into (4.3) and substituting into (4.10) we obtain

$$J_P\simeq\alpha\frac{\hbar^2}{2m}\frac{(V_0)^{1/2}(L)}{g}\exp\left[-\frac{2}{g}\int_0^L(V_0)^{1/2}(\theta)d\theta\right] , \tag{4.13}$$

where

$$\alpha=\prod_{i=1}^{N-1}\int_0^\infty d\eta_i\exp\left[-\frac{[V_2^{ii}(L)]^{1/2}}{\sqrt{2}g}\eta_i^2\right]\Big/\int_v\psi^2dv \tag{4.14}$$

represents the effective area of the section of the wave function by the $(3N-1)$-dimensional hyperplane Σ.

The main contribution to the integral in the denominator comes from the regions close to the equilibrium configuration X_I. One can consider a reference frame $(\vec{\theta}',\vec{\eta}'_i)$ parallel to $(\vec{\theta},\vec{\eta}_i)$ and centered at X_I. In this frame, a crude approximation of ψ is

$$\psi \simeq \Phi(\theta) \prod_{i=1}^{N-1} \exp\left[-\frac{[V_2^{ii}(0)]^{1/2}}{2\sqrt{2}g} \eta_i'^2 \right],$$

where $V_2^{ii}(0)$ represents the second derivative of V^{12} at the cavity center $X_I(\theta=0)$,

$$V_2^{ii}(0) = \left[\frac{\partial^2 V^{12}}{\partial \eta_i'^2} \right]_{\vec{\rho}=X_I} .$$

Integrating the Gaussian factors we find

$$\alpha = \prod_{i=1}^{N-1} \left[\frac{V_2^{ii}(0)}{V_2^{ii}(L)} \right]^{1/4} \Big/ \int \Phi^2(\theta) d\theta . \tag{4.15}$$

Apart from a multiplicative factor

$$\alpha_\perp = \prod_{i=1}^{N-1} \left[\frac{V_2^{ii}(0)}{V_2^{ii}(L)} \right]^{1/4} , \tag{4.16}$$

we are led to a *one-dimensional* problem of tunneling along a curved path $\mathscr{L}(\theta)$ with potential $V_0(\theta)$.

The factor $\alpha_\perp$ is independent of g (within this rough approximation) and J_P is dominated by the exponential factor

$$\exp\left[-\frac{2}{g} \int_0^L (V_0)^{1/2}(\theta) d\theta \right] = \exp\left[-\frac{1}{g} \int_{X_I}^{X_P} (V_0)^{1/2}(\theta) d\theta \right]$$

(we use the symmetry of the path with respect to the median hyperplane Σ to write the second member). We find again the result expressed in Sec. III, relation (3.10). We have not searched to evaluate $\alpha_\perp$ exactly, but we can estimate its order of magnitude.

As we shall see in the following, in the critical exchange configurations, the distances between the particles are reduced by no more than $x \simeq 10$–15%, and the total number of coordinates for which the available space is appreciably reduced is of the order of $n_r \simeq 6$–10; hence, $\alpha_\perp$ might be of the order of

$$[(1-x)^{14}]^{n_r/4} \simeq 10^{-1} - 10^{-2} . \tag{4.17}$$

(ii) Higher orders in g: the next orders in g [see Sec. IV A 2, Eqs. (4.7) and (4.8)] lead to a constant and a term in $g^{1/5}$ in the exponent of J_P.

2. *With the 1/r Coulomb potential*

In reduced coordinates $\vec{\rho}$ the Schrödinger equation is

$$-\frac{\hbar^2}{2ma^2} \Delta\psi(\vec{\rho}) + \frac{1}{4\pi\epsilon_0} \frac{e^2}{a} \sum_{\substack{i,j=1 \\ i<j}}^{N} |\vec{\rho}_{ij}|^{-1} = E\psi(\vec{\rho}) . \tag{4.18}$$

Here, the quasiclassical limit applies at large interatomic distances when the kinetic energy decreasing in $1/a^2$ becomes smaller than the potential energy decreasing in $1/a$. We also choose as a parameter in the WKB series expansion the square root of the ratio of the kinetic-energy to potential-energy terms (i.e., the ratio of the Bohr radius $a_B = \hbar^2 4\pi\epsilon_0/me^2$ to the lattice spacing a),

$$g = (1/\sqrt{2})(a_B/a)^{1/2} . \tag{4.19}$$

At lowest order in g we obtain the same relation (4.13) of the preceding paragraph with g given by (4.19) and V^{12} being replaced by $V^1 = \sum_{i<j} |\vec{\rho}_{ij}|^{-1}$.

B. Determination of the exchange path (MPEP)

For a realistic comparison of two-, three-, four-, etc., spin-exchange frequencies we need to consider the $\nu = 2,3,4,\ldots,$ exchanging particles and a reasonable number of their neighbors which move away to favor the exchange. We take in each case about $N=16$ particles. The problem of finding a classical path in a $(3\times 16 = 48)$-dimensional space is not straightforward. We proceed by successive approximations in the following way.

1. *"Elementary" approximation*

a. Sinusoidal potential. The potential $V(t)$ along the exchange path is approximated to its first Fourier component,

$$V(t) - E_0 = \tfrac{1}{2} V_M [1 - \cos(\pi t/L)] . \tag{4.20}$$

t is chosen as the one-dimensional variable measuring the length along the path with $t=0$ at X_I and $t=L$ at X_M ($2L$ represents the total length of the exchange path). $V_M = V(X_M)$ is the value of the potential at X_M.

Within this simple approximation, the action

$$S = \int_{X_I}^{X_M} [2m(V-E)]^{1/2} dt$$

is straightforwardly calculated:

$$S = (2/\pi)(V_M)^{1/2} L .$$

As seen in the preceding paragraph, apart from a factor α_T representing an effective area for the section of the wave function by the $(3N-1)$-dimensional median hyperplane Σ, the exchange frequency is that corresponding to one-dimensional tunneling along a path $\mathscr{L}(t)$ with potential $V(t)$. The solutions of the Schrödinger equation with a sinusoidal potential $V(t)$ are Matthieu functions (see, for example, Ref. 20). Using the asymptotical relation (20.2.31) of Ref. 20 (valid in the small exchange limit), we write

$$J_P = \alpha_\perp 4\sqrt{2} \frac{\hbar^2}{2m(La)^2} \left[\frac{(V_M)^{1/2} L}{g} \right]^{3/2} \times \exp\left[-\frac{4}{\pi} \frac{(V_M)^{1/2} L}{g} \right] \tag{4.21}$$

[$\alpha_\perp$ is roughly estimated by the relation (4.16)].

b. Approximation of the path length. The length L is approximated to the length of the straight line joining X_I to X_M in the $3N$-dimensional configuration space,

$$L = \left[\sum_{i=1}^{N} (\delta\vec{\rho}_i)^2 \right]^{1/2} , \tag{4.22}$$

where $\delta\vec{\rho}_i$ represents the displacement of the ith particle.

c. Search for the optimum path. We have to search on Σ for the configuration X_M which minimizes the action $S=(2/\pi)(V_M)^{1/2}L$.

The median hyperplane Σ is defined by the equation

$$\sum_i(\vec{r}_i-\vec{R}_i)^2=\sum_i(\vec{r}_i-\vec{R}_{n_i})^2=0,\quad n_i=P(i) \tag{4.23}$$

which simply means that $X_M=(\vec{r}_1,\ldots,\vec{r}_N)$ on Σ is equidistant from the configurations X_I and X_P defined in Sec. III. This relation can be expressed in a simpler way:

$$\sum_i \vec{r}_i\cdot(\vec{R}_i-\vec{R}_{n_i})=0\ . \tag{4.24}$$

We are led to find the minimum of a function S of $3N$ variables $(r_1,\ldots,\vec{r}_N)$ submitted to the condition (4.24). We use a "steepest descent" method, proceeding in the following way:

(i) We start with a small number of moving particles (only the exchanging particles) and find an optimum configuration.

(ii) We successively add the nearest neighbors of the moving atoms in the critical exchange configuration X_M obtained at the preceding step and run the minimization process again. We iterate the process, adding more particles each time.

(iii) We stop when taking new moving neighbors does not change appreciably the minimum of S. We generally end with $N\simeq 16$ particles (i.e., ~ 48 variables).

2. Exact calculation

We cut the exchange path into n segments and evaluate the action S through a straightforward trapezoidal integration formula. We apply the same steepest descent method for minimization.

We consider n equidistant $(3N-1)$-dimensional hyperplanes Σ_k defined by

$$\sum_i(\vec{r}_i-\vec{R}_{\nu_i})^2-\sum_i(\vec{r}_i-\vec{R}_i)^2=\frac{d^2}{n}k,\quad \nu_i=P(i) \tag{4.25}$$

where d represents the distance between X_I and X_P (Σ_0 corresponds to the median hyperplane Σ, and Σ_n to the hyperplane parallel to Σ and passing through X_I).

We take one configuration X_k on each hyperplane Σ_k. The exchange path is approximated by the jagged line $X_IX_{n-1}\cdots X_1X_M$, and the action is evaluated through the trapezoidal formula

$$S=\sum_{k=0}^{n}\tfrac{1}{2}\{[\delta V(X_k)]^{1/2}+[\delta V(X_{k+1})]^{1/2}\}\,|X_kX_{k+1}|\ , \tag{4.26}$$

with $X_n=X_I$ and $\delta V(X_k)=V(X_k)-V(X_I)$ [we take $E_0\simeq V(X_i)$]. $|X_kX_{k+1}|$ denotes the distance between X_k and X_{k+1}.

We start from the configuration obtained within the straight-line approximation (1) with $X_0=X_M$, and

$$X_k=X_M+k(X_I-X_M)/n$$

(we recall that the X_k's are vectors in $3N$-dimensional configuration space).

We apply the steepest descent method with $3Nm$ variables to find the minimum of S. With $m=5$ and $N=16$ (240 variables), the minimization takes about one hour of CPU (central processing unit) time.

As we shall see in the following, for two-particle exchange this exact calculation leads to an improvement of the order of 10% in the value of S when compared to the "elementary" approximation (1). For higher-order (more symmetrical) exchanges, the two methods give the same S within less than 2%; therefore the elementary approximation can be considered as sufficient.

C. Results with various potentials in the two-dimensional triangular lattice

We begin with the simplest two-dimensional case (triangular lattice) and compare two-, three-, and four-particle exchange with three different potentials: (i), $1/r^{12}$ potential; (ii), full Lennard-Jones potential; (iii), $1/r$ Coulomb interaction. In all cases, three-particle exchange dominates; this feature seems to be a characteristic of the lattice geometry.

1. With the repulsive part of the Lennard-Jones potential: $V=4\epsilon(\sigma/r)^{12}$

We use the high-density series expansion in a/σ described in Sec. IV A. This calculation applies for a two-dimensional adsorbed layer of ^{3}He at high coverage.

a. Results within the sinusoidal approximation are presented as follows.

(i) Exchange frequencies for a small number of particles ($\nu\lesssim 6$). The results of the sinusoidal approximation described in Sec. III B 1 are compared in Figs. 1(a), 1(b), 1(c), 1(d), and 1(e), respectively, for $\nu=3$, 4, 6, 2, and 12 particles (we adopt a classification corresponding to the hierarchy obtained between various exchange frequencies). These figures show the particle positions in the critical exchange configuration X_M on Σ. The particle displacements are given numerically (in units of a), within the (X,Y) frame at the upper part of each figure. We also indicate the symmetry elements of each figure.

At the lower part of each figure we give the number N of moving atoms, the maximum $V=V_M$ of the potential on the median hyperplane Σ, the square of the path length

$$L^2=\sum_{i=1}^{N}(\delta\vec{\rho}_i)^2\ ,$$

and the product $\sqrt{V}\,L$. Within our reduced units all these quantities are dimensionless. The exchange frequency is, according to (4.21),

$$J_P\sim\alpha_P\exp(-S_P/g)\ , \tag{4.27}$$

with

$$S_P=\frac{4}{\pi}\sqrt{V}\,L\quad\text{and}\quad g=\frac{\hbar}{(8m\sigma^2\epsilon)^{1/2}}\left[\frac{a}{\sigma}\right]^5\ .$$

In Fig. 2 we show for $\nu=3$ exchanging particles the

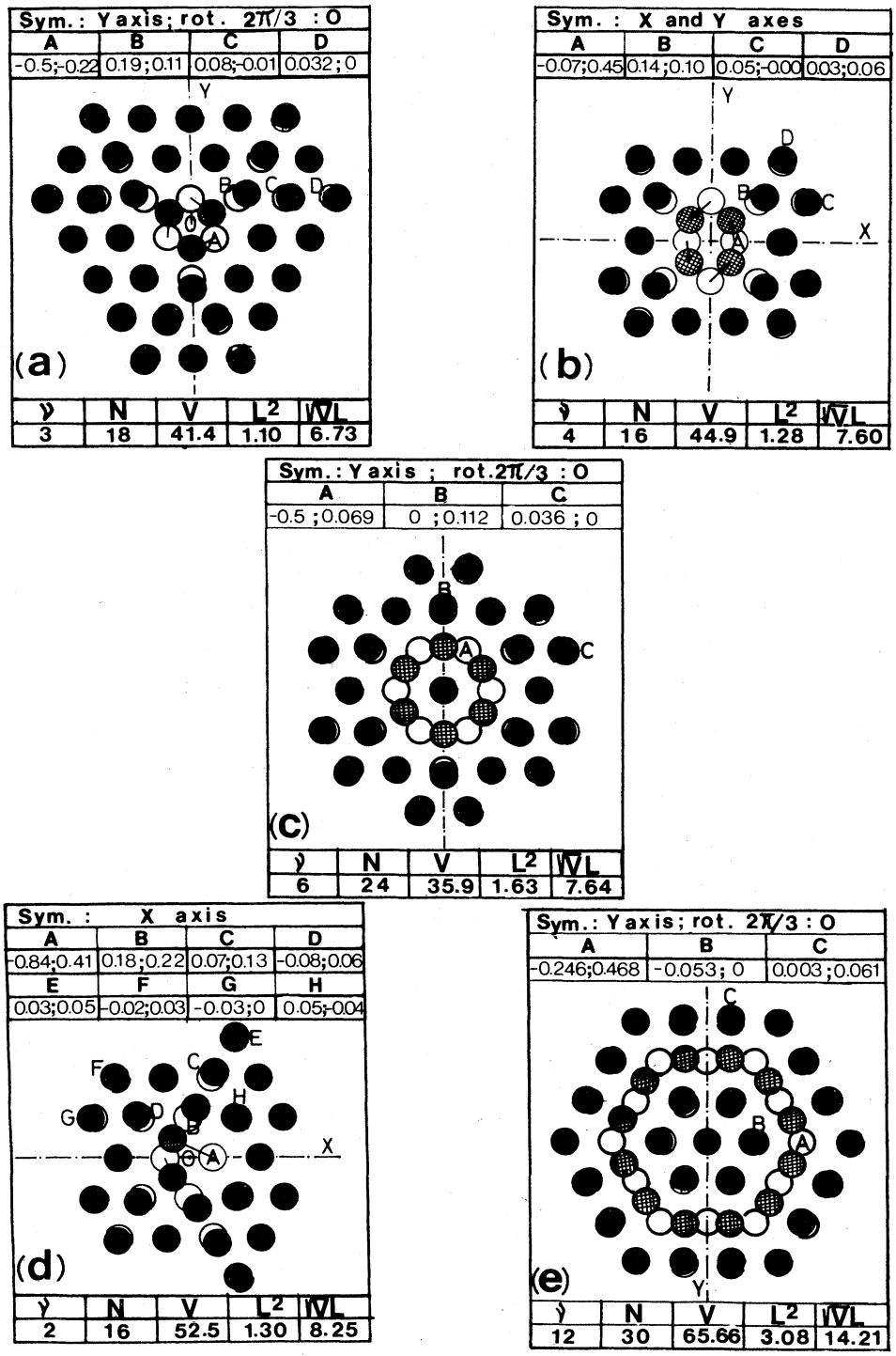

FIG. 1. Multiple-exchange processes in the 2D lattice with $(1/|\rho|)^{12}$ potential. The exchange processes are classified (a)—(e) by decreasing order of magnitude. The open circles represent the equilibrium positions. The atom positions in the critical exchange configuration (on the median hyperplane Σ between the two permuted equilibrium configurations) are represented by cross-hatched (exchanging atoms) and solid circles (neighboring atoms). The symmetry elements of the figures are indicated at the upper part with the displacements of the particles in the orthonormal X, Y frame, in units of a (interatomic spacing). Below each figure we give the number ν of exchanging particles, the number N of moving atoms, the height $V = V_M$ of the potential barrier, the square of the exchange path half-length L, and the product $\sqrt{V}\,L$ which determines the exponent in J_P. The unit for L is a, and $V = \sum_{ij}(a/|\rho_{ij}|)^{12}$ is dimensionless.

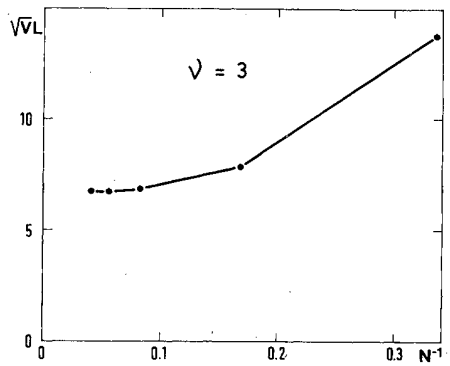

FIG. 2. Exponent $\sqrt{V}L$ for three-particle exchange as a function of $1/N$ (N represents the number of moving atoms). At least 12 atoms are needed to obtain a reliable value.

evolution of $\sqrt{V}L=(\pi/4)S_P$ in terms of the number N of moving atoms. It proves that a number of $N\simeq 12-18$ moving particles at least is required to obtain S_P. The same conclusion holds for each ν (the details are not reported).

Three-particle exchange clearly dominates with $S_3=8.57$. Afterwards come cyclic four- and six-particle exchanges with about the same action ($S_4\simeq 9.67$ and $S_6\simeq 9.72$); the length of the exchange path is shorter for four-particle exchange $L=1.13$ (compared to 1.28 for $\nu=6$), but the potential is higher, $V=44.9$ for $\nu=4$ (compared to $V=35.9$ for $\nu=6$). Close behind follows two-particle exchange with $S_2=10.50$; two-particle exchange involves a large displacement of the surrounding particles, leading to a length $L=1.14$ practically equal to that corresponding to the four-particle exchange process. The critical configuration is not symmetric with respect to the Y axis. Instead of a symmetrical block rotation of the pair, the system prefers the "vacancy-interstitial" configuration of Fig. 1(d), which increases the length L but lowers the potential barrier. Owing to this disymmetry, the number of equivalent exchange paths is $s=4$ compared to $s=1$ for all other exchange processes ($\nu=3,4,6,\ldots$). This leads to a factor 4 in the expression of the pair exchange frequency J_2. However, at very high density the exponential factor dominates and the hierarchy of the different exchange frequencies is unaffected by s. In conclusion, the competition between the height V_M of the tunneling barrier and the length of the exchange path L leads to the following hierarchy for the most compact cyclic ν-particle exchange frequencies J_ν,

$$J_3>J_4\sim J_6>J_2\ .$$

(ii) Behavior of the exchange frequency for large ν. The exchange model would be meaningless if we had no argument that for large ν, J_ν decreases monotonically and rapidly. We have investigated the most symmetric 12-atom exchange [Fig. 1(e)]. As for six-particle exchange, the critical configuration corresponds to a block rotation of the exchanging particles. The potential barrier is twice that obtained for six-particle exchange. The square path length $L^2=3.08a^2$ corresponds practically to $\nu(a/2)^2$. Hence, we expect, for highly symmetric exchanges with $6<\nu<12$ particles, a potential barrier proportional to ν, a length L proportional to $\sqrt{\nu}$, and a rapid decrease of J_ν as $\exp(-\text{const}\times\nu)$. For very large ν ($\nu\gtrsim 15$ to 20), as shown in the Appendix, exchange via the creation and separation of a pair vacancy interstitial will become more favorable. The potential barrier (representing the energy for the creation of a pair vacancy interstitial) will become independent of ν and exchange will decrease more slowly, as $\exp(-\text{const}\times\sqrt{\nu})$.

b. Exact calculation. We have performed the calculation described in Sec. IV B 2 with $m=5$ for two- and three-particle exchange. The configurations corresponding to the five points X_0 to X_4 are shown in Figs. 3(a) and 3(b), respectively, for two- and three-particle exchange. On Figs. 4(a) and 4(b) the lengths of the successive segments X_kX_{k+1} of the exchange path have been represented in the following schematic way: the equidistant hyperplanes Σ_k are represented by parallel vertical lines. The part of the exchange path between two hyperplanes Σ_k

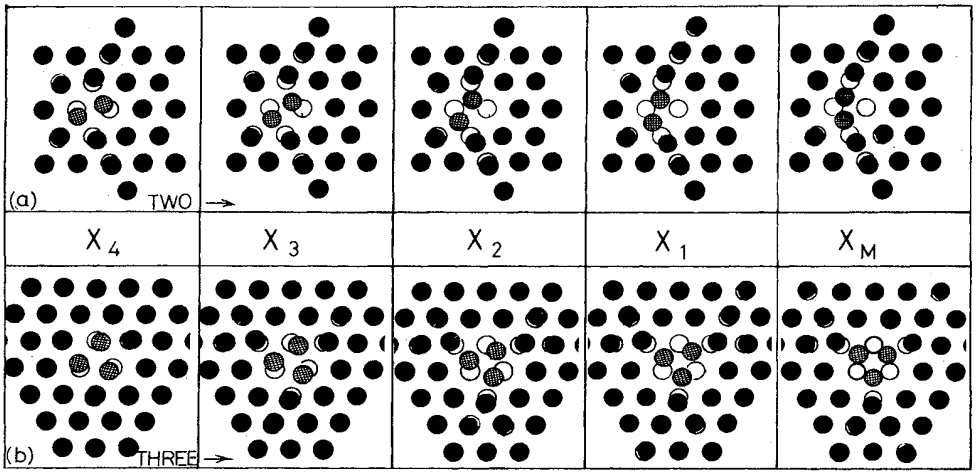

FIG. 3. "Cinematographic" view of (a) two- and (b) three-particle exchange. Five configurations corresponding to five points X_k of the exchange path situated on five equidistant hyperplanes Σ_k are shown. The convention for the representation of the particles is the same as in Fig. 1.

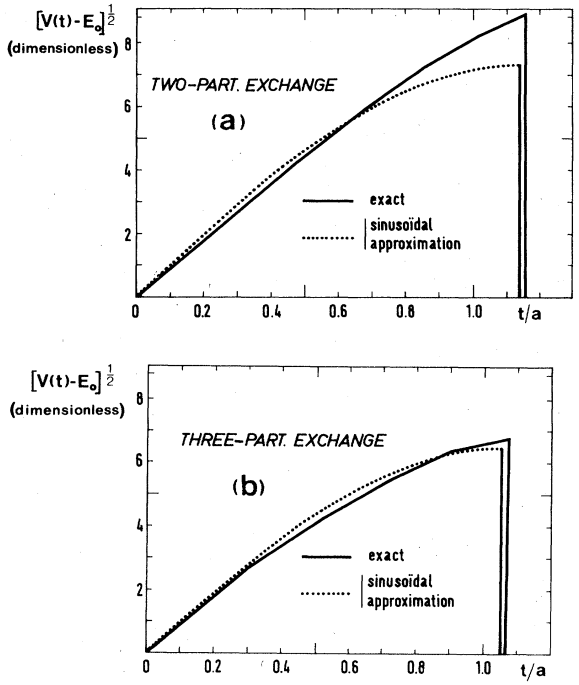

FIG. 4. Square root $[V(t)-E]^{1/2}$ of the potential along the exchange path (solid curve) is compared with the sinusoidal approximation (dotted line): (a) for pair exchange; (b) for three-particle exchange. The sinusoidal approximation is remarkably good in the second case.

and Σ_{k+1} is figured by a segment of length $|X_kX_{k+1}|$. In Figs. 5(a) and 5(b) we compare the values of the potential at X_k with the sinusoidal approximation.

For two-spin exchange this improved method leads to $S_P=11.26$ and $L=1.15$ (compare to $S_P=10.50$ and $L=1.14$ within the elementary approximation). For three-spin exchange we obtain $S_P=8.65$ and $L=1.07$ (instead of $S_P=8.57$ and $L=1.05$ in the elementary approximation).

TABLE I. Multiple exchange in the two-dimensional triangular lattice with full Lennard-Jones potential $V=4\epsilon[(\sigma/r)^{12}-(\sigma/r)^6]$ with $r/\sigma=2^{1/6}$. Comparison of barrier height V, path length L, and action $S_P\sim\sqrt{V}\,L$ for $\nu=3$, 6, 4, and 2 exchanging particles.

	V_m	L^2	$(V_M)^{1/2}L$
Three particle	19.96	1.15	4.79
Six particle	16.67	1.64	5.23
Four particle	22.45	1.32	5.44
Two particle	23.57	1.43	5.80

Our elementary approximation underestimates S_P within 8% for two-particle exchange. It is particularly accurate for three-particle exchange and gives S_P within 1%. We expect from this method the same accuracy for higher-order exchange frequencies. We shall consider it as sufficient for $\nu>2$ exchanging particles.

2. *Results with the full Lennard-Jones potential: $V=4\epsilon[(\sigma/r)^{12}-(\sigma/r)^6]$*

In this subsection the mass is assumed to be large and the WKB series is written with expansion parameter $\hbar/\sqrt{m}$. The interatomic spacing a is chosen to correspond to the minimum of the Lennard-Jones potential, $a=a_0=2^{1/6}\sigma$. Note that for rare gases heavier than He, the density of a complete monolayer adsorbed on a substrate corresponds practically to $a=a_0$ (see, for example, Ref. 21).

The position of the atoms in the critical exchange configuration are practically those of Fig. 1 with slightly larger displacements. Table I shows the values of V_M, L^2, and $\sqrt{V}L$ for $\nu=2$, 3, 4, and 6 exchanging particles. The lengths are still expressed in reduced units with respect to a_0. V_M is dimensionless and the exchange frequency is

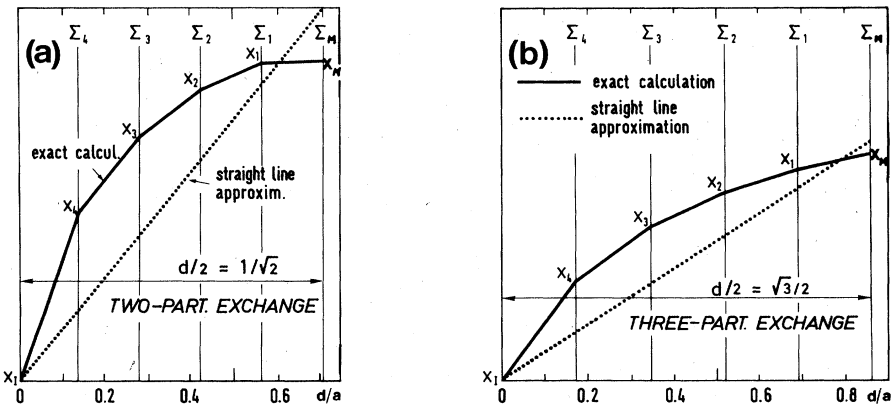

FIG. 5. Image of the exchange path. Five equidistant hyperplanes Σ_k are represented by vertical lines. Distance between the centers of the two cavities is d; distance between two consecutive hyperplanes Σ_k and Σ_{k+1} is $d/(2\times5)$. The segment X_kX_{k+1} represents the length of the exchange path between two consecutive hyperplanes. The dotted line represents the length of the exchange path within the straight-line approximation ($L=[\sum_{i=1}^{N}(\vec{\delta\rho}_i)^2]^{1/2}$). (a) represents two-particle exchange; (b) represents three-particle exchange.

$$J_v \sim \exp\left[-\frac{(8m\sigma^2\epsilon)^{1/2}}{\hbar}\left[\frac{\sigma}{a_0}\right]^5 (V_M)^{1/2}L\right]. \quad (4.28)$$

The hierarchy obtained is practically the same as in Sec. IV C 1 with dominant three-spin exchange; then come six- and four-particle exchanges with the same order of magnitude. Pair exchange is still smaller.

3. *Exchange with the Coulomb interaction potential (Wigner solid)*

As explained in Sec. IV A 2, we determine the first terms of a low-density series expansion in $1/a$. We use the same methods as in the preceding subsections, IV C 1 and IV C 2, with some complications due to the divergence of the $1/r$ sums.

(i) The interaction energy $E_I(\vec{r})$ of one electron at position $\vec{r}$ with all other electrons fixed at the lattice sites $\vec{R}_l$ ($l\neq 0$) is determined with the aid of the usual Ewald transformation. We use the integral representation

$$\frac{1}{|\vec{r}-\vec{R}_l|} = \frac{2}{\sqrt{\pi}}\int_0^\infty du\, e^{-u^2|\vec{r}-\vec{R}_l|^2}, \quad (4.29)$$

and the Ewald generalized θ-function transformation in two dimensions,[22]

$$\sum_l \exp(-u^2|\vec{r}-\vec{R}_l|^2) = \frac{\pi}{su^2}\sum_{\vec{G}}\exp(i\vec{G}\cdot\vec{r})\exp\left[-\frac{|\vec{G}|^2}{4u^2}\right]. \quad (4.30)$$

$s=a^2\sqrt{3}/2$ is the area of the unit cell and the sum $\sum_{\vec{G}}$ is extended to all vectors $\vec{G}$ of the reciprocal lattice.

We use the usual separation of the Ewald method,[22]

$$\sum_l \frac{1}{|\vec{r}-\vec{R}_l|} = 2\frac{\sqrt{\pi}}{s}\sum_{\vec{G}}\exp(i\vec{G}\cdot\vec{r}) \times\int_0^\epsilon \frac{1}{u^2}\exp\left[-\frac{|\vec{G}|^2}{4u^2}\right]du + \frac{2}{\sqrt{\pi}}\sum_l\int_\epsilon^\infty e^{-u^2|\vec{r}-\vec{R}_l|^2}du, \quad (4.31)$$

the right-hand side of (4.31) being independent of ϵ. With obvious variable changes both integrals in (4.31) can be expressed in terms of the function

$$\phi(Z)=\sqrt{\pi}\,\mathrm{erfc}(Z)/Z, \quad (4.32)$$

where erfc(Z) denotes the complementary error function,

$$\mathrm{erfc}(Z)=\frac{2}{\sqrt{\pi}}\int_Z^\infty e^{-u^2}du.$$

We write:

$$\sum_l \frac{1}{|\vec{r}-\vec{R}_l|} = \frac{\sqrt{\pi}}{s\epsilon}\sum_{\vec{G}}\phi(|\vec{G}|/2\epsilon)\exp(i\vec{G}\cdot\vec{r}) + \frac{\epsilon}{\sqrt{\pi}}\sum_l\phi(\epsilon|\vec{r}-\vec{R}_l|). \quad (4.33)$$

The interaction energy

$$E_I(\vec{r})=\sum_{l\neq 0}1/|\vec{r}-\vec{R}_l|$$

is obtained by subtracting $1/|\vec{r}|$ from the preceding relation, (4.33):

$$E_I(\vec{r})=\frac{\sqrt{\pi}}{s\epsilon}\sum_{\vec{G}}\phi(|\vec{G}|/2\epsilon)\exp(i\vec{G}\cdot\vec{r}) + \frac{\epsilon}{\sqrt{\pi}}\sum_{l\neq 0}\phi(\epsilon|\vec{r}-\vec{R}_l|) + \left[\frac{\epsilon}{\sqrt{\pi}}\phi(\epsilon|\vec{r}|)-\frac{1}{|\vec{r}|}\right]. \quad (4.34)$$

We note that (4.33) and (4.34) contain one divergent term, $(1/|\vec{G}|)_{\vec{G}=\vec{0}}$.

It is easily proved that the last term in the large parentheses tends to a constant $-2\epsilon/\sqrt{\pi}$ when $|\vec{r}|\to 0$. If we are only interested in calculating energy differences, $\Delta E_I(\vec{r})=E_I(\vec{r})-E_I(0)$, the divergent term in $1/|\vec{G}|$ disappears:

$$\Delta E_I(\vec{r})=\frac{\sqrt{\pi}}{s\epsilon}\sum_{\vec{G}\neq 0}\phi(|\vec{G}|/2\epsilon)[\cos(\vec{G}\cdot\vec{r})-1] + \frac{\epsilon}{\sqrt{\pi}}\sum_{l\neq 0}[\phi(\epsilon|\vec{r}-\vec{R}_l|)-\phi(\epsilon|\vec{R}_l|)] + \frac{\epsilon}{\sqrt{\pi}}\phi(\epsilon|\vec{r}|)-\frac{1}{|\vec{r}|}+\frac{2\epsilon}{\sqrt{\pi}}. \quad (4.35)$$

Following Ref. 23 we take the separation $\epsilon=(\pi/s)^{1/2}$ which symmetrizes the roles of the sums over $\vec{G}$ and $\vec{R}_l$ in relation (4.35). Using the fact that the reciprocal lattice is obtained from the direct triangular lattice by a rotation of $\pi/2$ followed by the similarity of ratio $2\pi/s$, we write

$$\Delta E_I(\vec{r})=s^{-1/2}\sum_{l\neq 0}\left\{\left[\cos\left[\frac{2\pi}{s}(R_l^x r^y+R_l^y r^x)\right]-2\right]\phi\left[\left[\frac{\pi}{s}\right]^{1/2}\vec{R}_l\right]+\phi\left[\left[\frac{\pi}{s}\right]^{1/2}|\vec{r}-\vec{R}_l|\right]\right\} + \left[s^{-1/2}\left\{\phi\left[\left[\frac{\pi}{s}\right]^{1/2}|\vec{r}|\right]+2\right\}-\frac{1}{|\vec{r}|}\right], \quad (4.36)$$

where R_l^α and r^β are the components of $\vec{R}_l$ and $\vec{r}$ in the orthonormal (x,y) frame related to the direct lattice.

(ii) For N moving atoms, the energy difference ΔV between the equilibrium position ($\vec{r}_i=\vec{R}_i$) and a given configuration ($\vec{r}_i'=\vec{R}_i+\Delta\vec{r}_i$) is obtained from (4.36) by the following sum over the N displaced atoms:

$$\Delta V=\sum_{i=1}^{N}\Delta E_I(\Delta\vec{r}_i)$$
$$+\sum_{\substack{i,j=1\\ i<j}}^{N}(|\vec{r}'_i-\vec{r}'_j|^{-1}+|\vec{R}_i-\vec{R}_j|^{-1}$$
$$-|\vec{r}'_i-\vec{R}_j|^{-1}-|\vec{R}_i-\vec{r}'_j|^{-1}). \quad (4.37)$$

(iii) From the relations (4.36) and (4.37), the search for the exchange path and the exchange calculation are performed according to the method described in Sec. IV B.

From (4.13) and (4.21) we have

$$J_\nu=\alpha_\perp 4\sqrt{2}\frac{\hbar^2}{2m(La)^2}\left[\frac{(V_M)^{1/2}L}{g}\right]^{3/2}$$
$$\times\exp\left[-\frac{4}{\pi}\frac{(V_M)^{1/2}L}{g}\right], \quad (4.38)$$

where

$$g=\frac{1}{\sqrt{2}}\left[\frac{a_B}{a}\right]^{1/2};\quad a_B=\frac{\hbar^2 4\pi\epsilon_0}{me^2}$$

is the Bohr radius.

The particle configurations at the middle of the exchange path and the corresponding values of $V=V_M$ and L are given in Fig. 6 for $\nu=2$, 3, and 4 exchanging electrons:

$$V_M\simeq\sum_{i>j}a/|\vec{r}_i-\vec{r}_j|$$

is dimensionless; the length unit for L is a.

Three-particle exchange still clearly dominates with $(V_M)^{1/2}L=0.68$. Then come two- and four-electron exchange with the same exponent, $(V_M)^{1/2}L\simeq 0.76$. There are significant differences in the critical exchange configurations, compared with the results obtained with the $1/r^{12}$ and the full Lennard-Jones potential.

(i) The displacements of the neighboring particles are reduced, and the lengths L of the exchange paths are smaller and increase monotonically with the number ν of exchanging electrons: $L=0.85$, 0.95, and 1.05 for $\nu=2$, 3, and 4, respectively.

(ii) The critical exchange configuration for pair exchange is symmetric with respect to the X and Y axes. [For a $1/r^{12}$ potential, the repulsion is stronger; consequently, the action $S_2\simeq(V_M)^{1/2}L$ is decreased by putting the exchanging particles in a disymmetrical configuration for which the length L is larger but the potential barrier V_M is much smaller.]

With dominant three-particle exchange, the two-dimensional Wigner solid will be ferromagnetic at least at low densities. This answers a question raised a long time ago. Herring[24] was the first author to point out that multiple-exchange effects could be important in the Wigner solid as well as in solid ^{3}He.

The two-dimensional Wigner solid has been observed for electrons on bulk liquid He or on He films adsorbed on solid neon. The highest densities reached are $\sim 10^9$ on liquid He (Ref. 25) and $\sim 10^{10}$ on thin He films adsorbed on neon (Ref. 26). The two-dimensional electron fluid is obtained at much higher densities in semiconductor inversion layers.

It is interesting to illustrate (4.38) with some numerical values. The Bohr radius is $a_B\simeq 0.53$ Å. Let us take $a=50$ Å$\sim 100a_B$ corresponding to a density of $4.6\times 10^{12}\ e/\text{cm}^2$. The parameter $g\simeq 0.073$ is sufficiently small, and we expect our quasiclassical limit to be still valid. For three-spin exchange in a free-electron surface, we obtain

$$J_3/k_B=2901\alpha_\perp\exp(-11.86)\ \text{K}\simeq 0.02\alpha_\perp\ \text{K}$$

($\alpha_\perp$ is of the order of 10^{-1} to 10^{-2}). Unfortunately, the electron densities now obtained at the surfaces of liquid He on neon are too low compared to the density we took

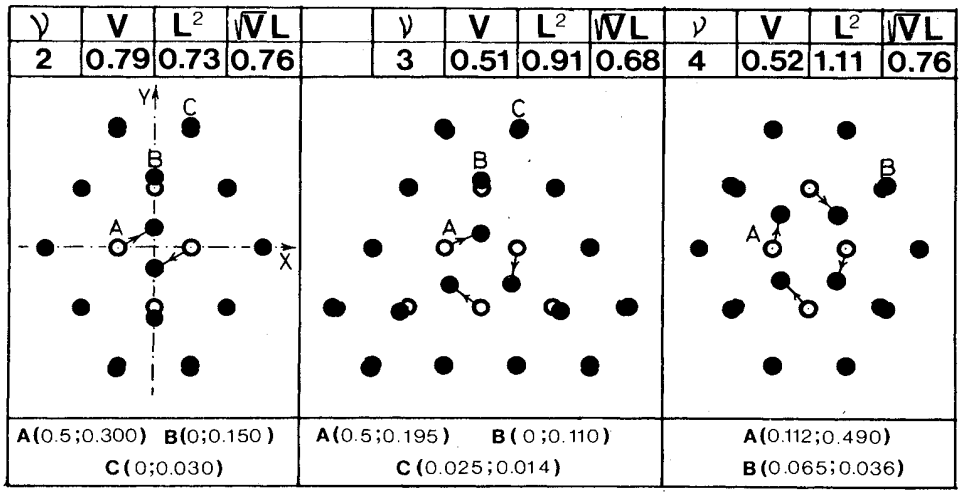

FIG. 6. Multiple exchange in the two-dimensional electron Wigner solid. The open and solid circles represent, respectively, the equilibrium and critical configurations for the electrons. The particle displacements are indicated (in the X, Y frame) below the figure. On the top we compare the potential barrier V (dimensionless), the square length of the path (units of a^2), and the action $\sqrt{V}\,L$.

in this example, and exchange effects are not measurable.

Much higher electron densities are obtained in semiconductor inversion layers.[27] Let us give some data for silicon. The effective mass is $m^*=0.2m$ and the dielectric constant is $\epsilon=8\epsilon_0$. Consequently, in the preceding formula the Bohr radius is replaced by

$$a_B^*\simeq 40a_B\simeq 21.2\ \text{Å}\ .$$

Let us take $a=2000$ Å corresponding to a density of $2.9\times10^9\ e/\text{cm}^2$; we have $g\simeq 0.073$ and

$$J_3/k_B\simeq 9\alpha_\perp \exp(-11.86)\ \text{K}\simeq \alpha_\perp 6.4\times10^{-5}\ \text{K}\ .$$

The usual minimum densities now obtained in silicon devices are of the order of $10^{12}\ e/\text{cm}^2$. For such densities the ratio g^2 of the kinetic-energy to potential-energy terms is of order 1 and the quantum fluctuations destroy the Wigner solid. Intermediate densities are needed to test our predictions.

4. Conclusion

In the two-dimensional triangular lattice we have found dominant three-particle exchange with various potentials. It seems that this property is essentially related to the lattice geometry and does not depend on the precise potential shape, provided it is repulsive.

D. Exchange in hcp solid ^{3}He

We now investigate the three-dimensional hcp lattice in the high-density limit with the $1/r^{12}$ potential. Even if we restrict our calculation to permutations involving only first neighbors, there are a lot of two-, three-, and four-particle exchange cycles in the hcp lattice.

1. Exchange in the basal planes

The arrangement of the atoms in a basal plane is triangular. First, we have to consider two-, three-, four-, and six-particle exchange in that plane. There are two kinds of three-particle exchange cycles, depending on the position of the nearest atoms in the upper and lower neighboring planes. We have

(The striped circles represent the exchanging atoms; the open circles represent the atoms of the neighboring planes.)

It is obvious that the atoms of the neighboring planes leave more free space for exchange in the first case, and we expect $J_T>J_T^*$. There is only one kind of two-particle exchange, J_2, and one kind of four-particle exchange, K_P. We also consider the most symmetric six-particle exchange, S_{IX}.

2. Exchange cycles out of the basal plane

We have one kind of two-particle exchange, J_2', and one kind of three-particle equilateral triangles, J_T'. There are six kinds of four-particle exchange cycles. Two are planar: one forms a square (K_{sq}') and the other a parallelogram (K_P'), and four are folded.

TABLE II. Comparison of barrier height V, path length L, and action $S_P\sim\sqrt{V}\,L$ for the most important kinds of two-, three-, and four-particle exchange in hcp ^{3}He. The exchange constants are classified by decreasing order. The primes refer to exchange cycles out of the basal plane.

	V_M	L^2	$(V_M)^{1/2}L$
J_T	53.7	1.00	7.33
J_T'	60	1.00	7.75
K_{sq}'	57	1.14	8.09
J_2'	79	0.935	8.60
J_T^*	76	1.02	8.83
K_P'	67	1.20	9.00
K_P	69	1.27	9.38
J_2	70	1.30	9.54

3. Results

We have investigated all these kinds of cycles. The results are summarized in Table II, in which the exchange frequencies are classified by decreasing order of magnitude. All folded four-particle exchanges and six-particle exchange are negligible [with $(V_M)^{1/2}L>9.75$]; the details are not reported.

Figures 7 and 8 represent the critical exchange configurations for the four-dominating processes. Three-particle exchange still dominates; triple exchange in the basal plane (J_T) is larger than out of the basal plane (J_T'); next comes square four-particle exchange (K_{sq}') and pair exchange (J_2') out of the basal plane.

It is interesting to estimate an order of magnitude of J_T/J_T' for the lowest densities of the hcp phase. In the high-density limit the exponents S_{J_T} and $S_{J_T'}$ differ by

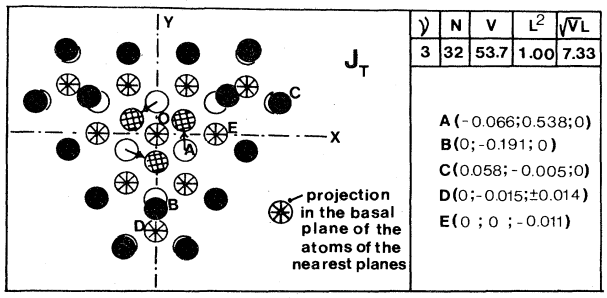

FIG. 7. Three-particle exchange J_T in the basal plane of the hcp lattice. The figure is invariant by rotation of $2\pi/3$ around the axis perpendicular to the basal plane and passing through 0. The open circles are the equilibrium positions. The exchanging atoms are the cross-hatched circles, and their neighbors in the basal plane are denoted by the solid circles. The starred circles represent the projection of the atoms of the upper and lower neighboring planes. The displacements of the atoms in an orthogonal X,Y,Z frame are indicated with respective units a,a,c; and $c=a\sqrt{8/3}$ is the height of the elementary cell.

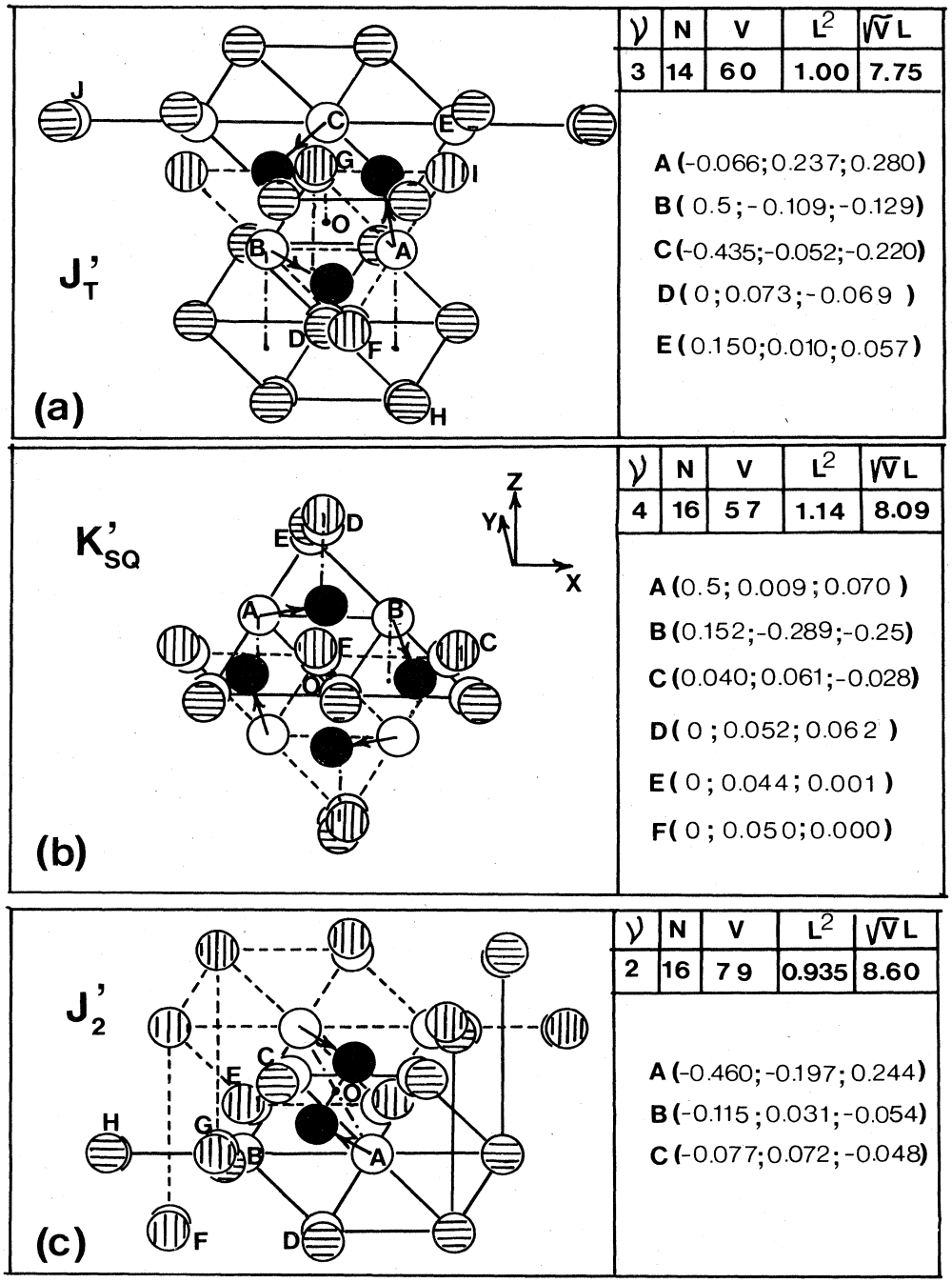

FIG. 8. (a) Three-, (b) square four-, and (c) two-particle exchange of the basal plane in the hcp lattice. The exchanging atoms are represented by solid circles. The open circles stand for the equilibrium configurations. The neighboring atoms in the critical configuration are striped circles; horizontal- and vertical-striped circles represent, respectively, atoms of successive planes parallel to a basal plane. (a) is invariant by symmetry with respect to the plane perpendicular to AB and passing through 0. (b) is invariant by symmetry with respect to the center 0 of the square and with respect to the plane perpendicular to AB and passing through 0. (c) is invariant by symmetry with respect to 0. For each exchange process, we compare the potential barrier V, the path length L (unit is the interatomic distance a) and the product $\sqrt{V}L$. The numbers in parentheses indicate the particle displacements in the orthogonal X,Y,Z frame with respect units $a,a,c=a\sqrt{8/3}$.

about 5.6%. Let us assume that this relative difference remains of the same order at lower densities. For $V=19.5$ cm^3/mol, the exchange frequency in hcp ^{3}He, obtained from nuclear magnetic resonance, is of the order of 2×10^{-2} mK. The Debye temperature is $\Theta_D\simeq30$ K. The order of magnitude of S is given by

$$J_T/k_B\simeq\Theta_D\exp(-S)\ .$$

The preceding values lead to

$$S \simeq \ln(k_B \Theta_D / J_T) \simeq 14 .$$

We conclude that

$$S_{J_T'} - S_{J_T} \simeq 14 \times 5.6 \times 10^{-2} \simeq 0.8$$

and

$$J_T / J_{T'} \simeq e^{0.8} \simeq 2 .$$

The same reasoning leads to $J_T / K'_{sq} \simeq 4$ and $J_T / J'_2 \simeq 10$. Hence, triple-exchange processes dominate.

A three-spin permutation $\mathscr{P}_{ijk}^{(\sigma)}$ can be expressed as a product of two transpositions,

$$\mathscr{P}_{ijk}^{(\sigma)} = \mathscr{P}_{ij}^{\sigma} \mathscr{P}_{jk}^{\sigma} ,$$

replacing the transposition operators $\mathscr{P}_{ij}^{\sigma}$ by their expressions in terms of the Pauli matrices,

$$\mathscr{P}_{ij}^{\sigma} = \tfrac{1}{2}(1 + \vec{\sigma}_i \cdot \vec{\sigma}_j) ,$$

and adding the inverse permutation, we obtain

$$\mathscr{P}_{ijk}^{(\sigma)} + (\mathscr{P}_{ijk}^{(\sigma)})^{-1} = \tfrac{1}{2}(\vec{\sigma}_i \cdot \vec{\sigma}_j + \vec{\sigma}_j \cdot \vec{\sigma}_k + \vec{\sigma}_k \cdot \vec{\sigma}_i) + C .$$

This relation proves that triple exchange leads to a Heisenberg Hamiltonian with nearest-neighbor interactions.

Now, we have to distinguish pairs of first neighbors in the basal plane from pairs out of the basal plane. Let us take a pair in the basal plane: it contributes to one cycle in the basal plane (J_T) and two distinct cycles out of the basal plane (J'_T). Now, a pair out of the basal plane contributes to four distinct cycles J'_T.

The effective Hamiltonian is

$$\mathscr{H} = -J_1 \sum_{i<j} \frac{\vec{\sigma}_i \cdot \vec{\sigma}_j}{2} - J'_1 \sum_{k<l}{}' \frac{\vec{\sigma}_k \cdot \vec{\sigma}_l}{2} \tag{4.39a}$$

where the sums $\sum$ and $\sum'$ extend, respectively, to pairs in the basal plane and out of the basal plane, and

$$J_1 = J_T + 2J'_T, \quad J'_1 = 4J'_T , \tag{4.39b}$$

and with $J_T / J'_T \simeq 2$ we have $J_1 / J'_1 \simeq 1$. Hence the anisotropy will be small at the lowest densities. It will increase with the density. This system has a positive Curie-Weiss temperature,

$$\Theta = 3(J_1 + J'_1) = 3(J_T + 6J'_T) . \tag{4.40}$$

Note that we have neglected square four-particle exchange K'_{sq}. Although it is smaller than triple exchange, it introduces some "frustration" and could lead to exotic ordered phases.

E. Results in a bcc lattice

At physical densities the kinetic energy of bcc ^{3}He is of the same order of magnitude as the potential energy, and the WKB expansion limited to the first terms is certainly unrealistic. However, it is interesting, from a theoretical point of view, to determine in this geometry the first terms of the high-density series expansion in a/σ and to compare various exchange frequencies in this hypothetical limit. As we have shown, in the two-dimensional lattice the hierarchy between the multiple-exchange constants is essentially related to the lattice geometry; we expect that the hierarchy found in bcc ^{3}He, in this theoretical high-density limit, remains unchanged at lower densities. We take as pair interaction V, the attractive part of the Lennard-Jones potential, $(\sigma/r)^{12}$

1. *"Elementary" approximation*

The results are compared in Figs. 9–11 for two-, three-, and four-particle exchanges; we also consider the most symmetric six-particle exchange (Fig. 12). Planar four-particle exchange (K_P) dominates with the minimum action, $S_{K_P} = -(4/\pi)\sqrt{V}\, L = 8.47$, and path length $L = 1.07$. We recall that the length unit is the distance between first neighbors a,

$$V = \sum_{i<j} (a / |\vec{r}_{ij}|)^{12} ,$$

is dimensionless and the exchange frequency is

$$J_P \sim \exp\left[-\frac{1}{g} S_P\right]$$

with g given by relation (4.2). Next comes three-particle exchange (J_t) with $S_3 = 9.27$ and $L = 1.06$. For both triple and planar four-spin exchange the exchanging atoms remain in the $(1\bar{1}0)$ plane, in the critical configuration [see Figs. 9(a) and 10]. Next comes two-particle exchange (J_{NN}) with action $S_2 = 9.78$ and length $L = 1.05$. It is important to note that since the critical exchange configuration (see Fig. 11) is less symmetric than for other exchange processes, the number of equivalent paths is larger. There are six configurations equivalent to that of Fig. 11, obtained by rotation of $2\pi/3$ around the $\langle 111 \rangle$ axis and symmetry with respect to 0; we can also interchange the labels of the two exchanging particles in the critical configuration. This leads to a factor of 12 for pair exchange instead of 1 for all other exchanges that we consider. Although we have not calculated carefully the prefactors α_T for J_t and J_{NN}, we think that they are both of the same order because the potential barriers are similar. Consequently, the symmetry factor might favor pair exchange at physical densities. The Monte Carlo calculation suggested in Sec. III would be the best way to determine the hierarchy between J_t and J_{NN} at low densities. After pair exchange comes six-particle exchange (S_{IX}) with action $S_6 = 10.13$ and path length $L = 1.26$. Last comes folded four-particle exchange (K_F) with action $S_{K_F} = 10.58$ and path length $L = 1.14$. Folded four-particle exchange is thus negligible compared to planar four-particle exchange. The reason is essentially geometric and can be seen easily by comparing Figs. 9(a) and 9(b). In the critical exchange configuration the number of pairs of atoms whose distance is appreciably reduced ($a' \simeq 0.9a$) is eight for planar four-particle exchange and 12 for folded four-particle exchange. The length of the exchange path is also larger in folded geometry.

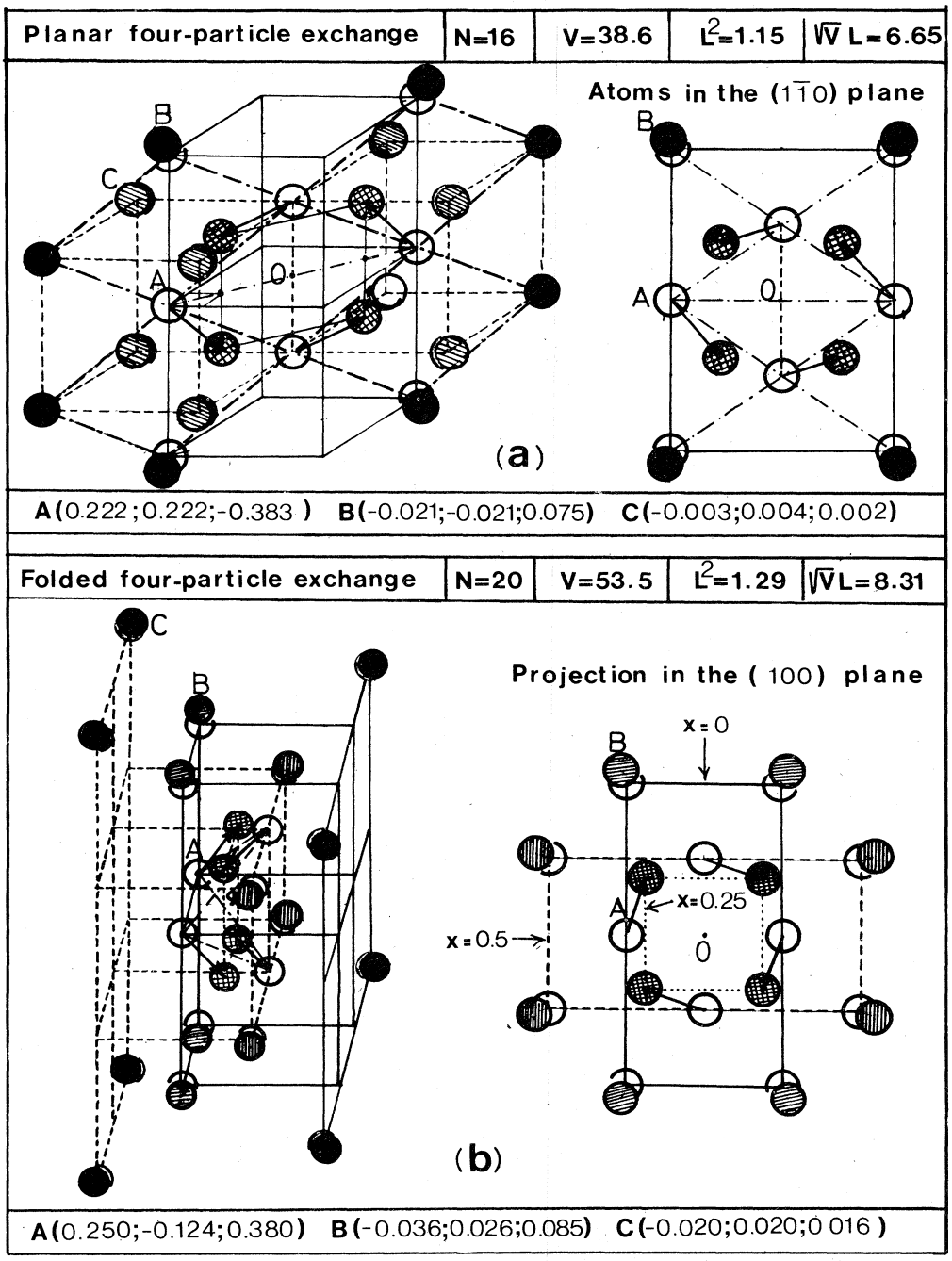

FIG. 9. Comparison of the two kinds of four-particle exchange in the bcc lattice: (a) planar four-particle exchange. Open circles represent the equilibrium configurations. The exchanging atoms are denoted by the cross-hatched circles, they remain in the (1$\bar{1}$0) plane, their neighbors in the same plane are represented by solid circles. The atoms in the neighboring parallel planes are simply striped circles. On the right-hand side we only represent the (1$\bar{1}$0) plane and the atoms that it contains. The figure is symmetric with respect to the (1$\bar{1}$0) plane and the (100) plane passing through 0. The atom displacements in an orthonormal X,Y,Z frame are indicated below the figure; the unit is the side $a=2a/\sqrt{3}$ of the conventional unit cube. (b) Folded four-particle exchange. Atoms in successive planes parallel to the (100) plane and corresponding to the abscissa $X=-0.5$, 0, 0.5, and 1 are, respectively, represented by solid, horizontal striped, vertical striped, and solid circles. The exchanging atoms (cross-hatched circles) are in a plane of abscissa $X=0.25$ parallel to the other planes. The figure on the right-hand side is a projection in the (100) plane. The (100) and (001) planes passing through 0 are symmetry planes. The figure is also invariant by a rotation of $\pi/2$ around the $\langle 100\rangle$ axis passing through 0, followed by a symmetry with respect to 0. It is clear from these figures (see in particular the projections) that the number of pairs of atoms whose distance in the critical configuration is appreciably reduced ($a'\simeq 0.85-0.9a$) is eight for planar four-particle exchange and 12 for folded four-particle exchange. Hence, the reason why planar four-particle exchange dominates is clearly geometric.

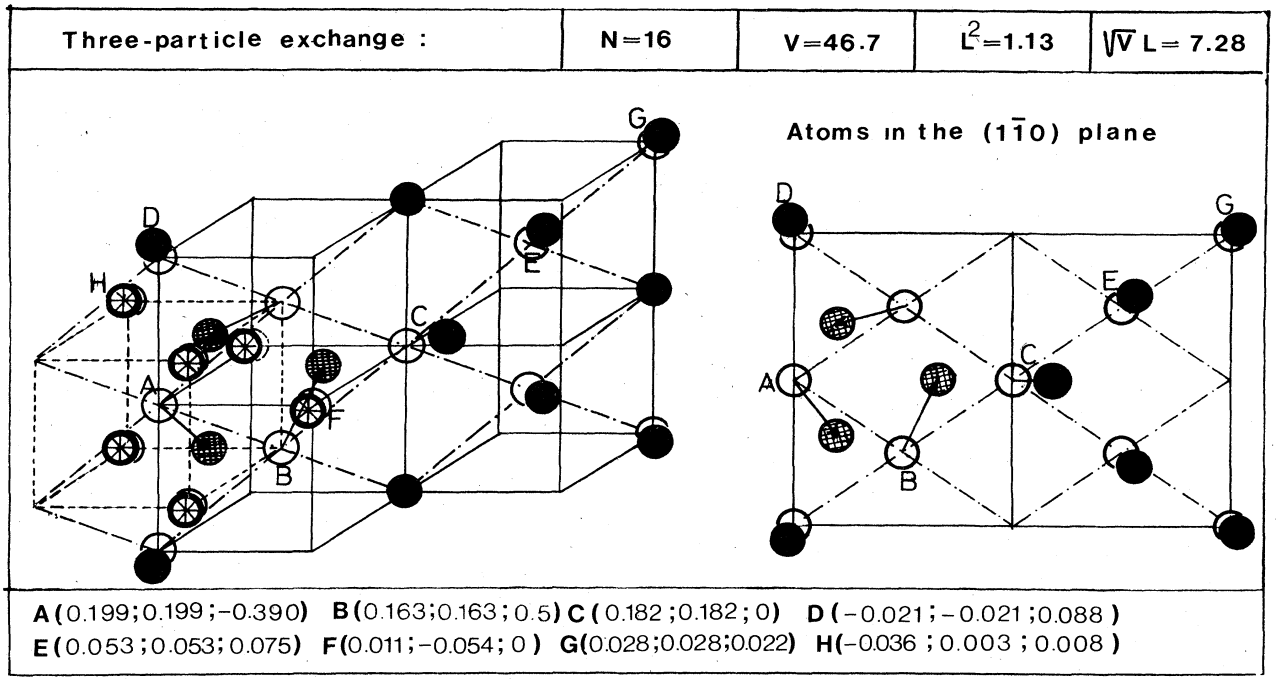

FIG. 10. Three-particle exchange in the bcc lattice. The open circles represent the equilibrium configurations. The exchanging atoms are denoted by the cross-hatched circles, their neighbors in the same (1$\bar{1}$0) plane are denoted by the solid circles. The atoms in the neighboring parallel planes are represented by starred circles. On the right-hand side of the figure we have represented the atoms in the (1$\bar{1}$0) plane. The figure is symmetric with respect to the (1$\bar{1}$0) plane and the (001) plane passing through C. The particle displacements (units of α) in the orthonormal X,Y,Z frame are indicated below the figure. Above the figure we give the number of moving particles N, the potential barrier V, and the square of the path length L^2.

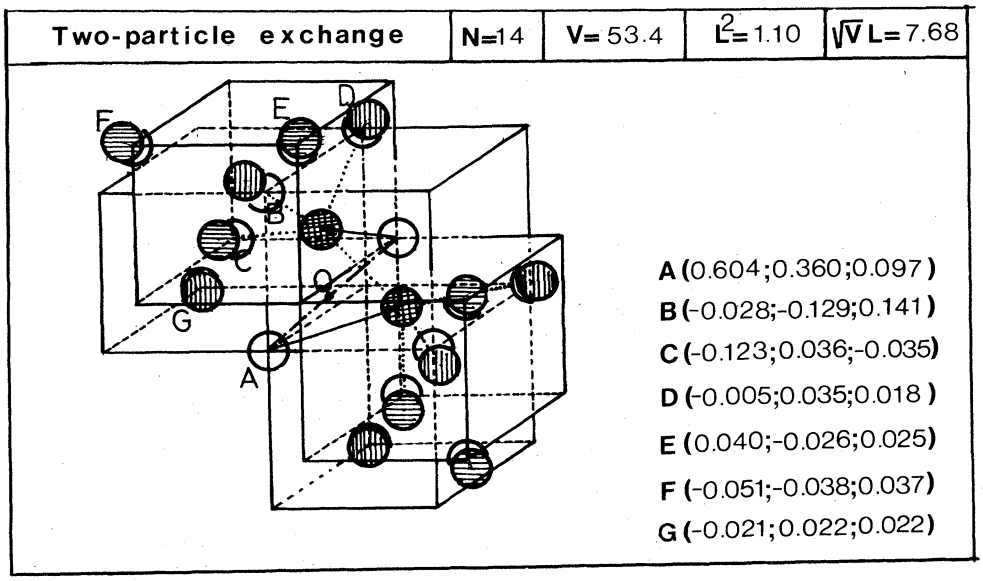

FIG. 11. Two-particle exchange in the bcc lattice. The bcc lattice is divided into two imbricated simple-cubic lattices. The atoms of these two sublattices are represented by, respectively, vertical- and horizontal striped circles. The exchanging atoms are denoted by the cross-hatched circles. The figure is invariant by symmetry with respect to the ($\bar{1}$01) plane passing through 0. We can obtain three equivalent configurations by rotation of $2\pi/3$ around the $\langle 111 \rangle$ axis, and, again, three other equivalent configurations by symmetry with respect to 0. Taking into account that we can also interchange the two particles in the critical configuration, we have 12 equivalent paths in $3N$-dimensional configuration space. For all other exchange processes that we consider in the bcc lattice, there is only one path. At physical densities, this factor of 12 might favor pair exchange with respect to triple exchange (although the action $S_P \sim \sqrt{V}\, L$ is smaller for three-particle exchange).

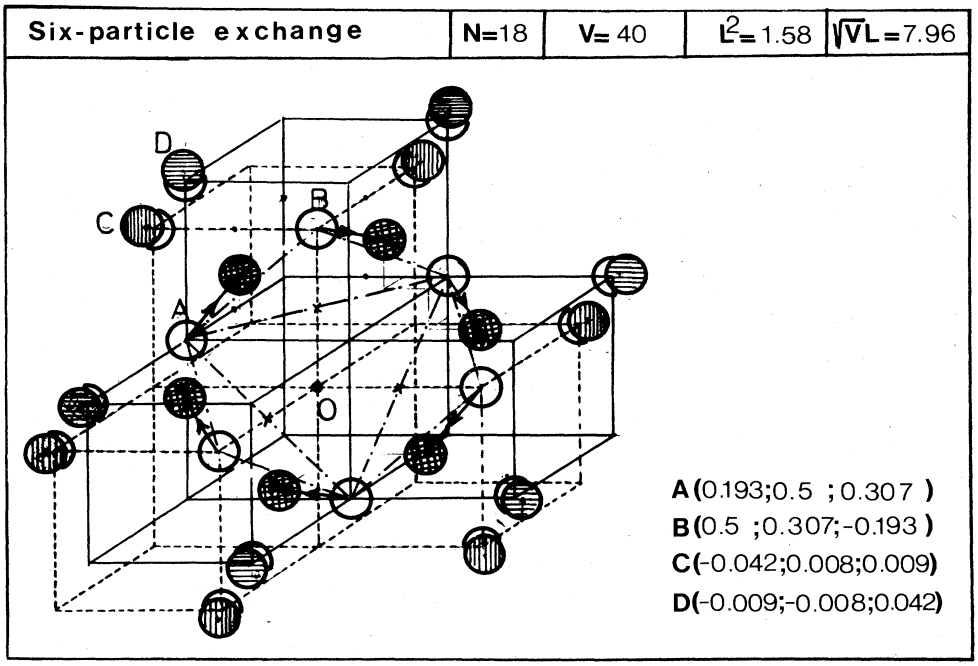

FIG. 12. Six-particle exchange in the bcc lattice. The particles are represented with the same conventions as in Fig. 11. The figure is invariant with respect to the rotation of $\pi/3$ around the $\langle 1\bar{1}1 \rangle$ axis passing through 0. Compared to folded four-particle exchange the length L is larger but the barrier height V is smaller and the product $\sqrt{V}\,L$ is also smaller, favoring six-particle exchange.

2. *Exact path determination*

In order to improve our comparison between triple and pair exchange we have performed the calculation described in Sec. IV B 2. The new results are $S_2=10.2$ for pair exchange with path length $L_2=1.076$ and $S_3=9.09$ for triple exchange with path length $L_3=1.10$. This calculation leads to a change of $+4\%$ in the exponent S_2 and of -2% in S_3; it increases the ratio $J_t/J_{\rm NN}$. Hence, $J_{\rm NN}$ is definitely smaller than J_t in the high-density limit. For more symmetric exchange (as four- and six-particle exchanges) we expect that the elementary approximation is sufficient and gives an accuracy better than 2% in the evaluation of the action S_P.

3. *Conclusion*

The hierarchy between various exchange frequencies given by the first terms of a high-density series expansion in a/σ is thus

$$K_P > J_t > J_{\rm NN} > S_{IX} > K_F \ . \tag{4.41}$$

This hierarchy corresponds strikingly to our assumptions in the model Hamiltonian used to fit the experimental data.[1] (We proposed a two-parameter Hamiltonian including only K_P and J_t with $J_t \simeq K_P/3$.) This is not surprising because we believe that the hierarchy given by (4.41) is essentially related to the lattice geometry and is not restricted to the theoretical high-density limit.

We note that this hierarchy does not correspond to that predicted by Avilov and Iordansky:[8] $J_{\rm NN} \gtrsim K_P \gg J_t$. We want to point out that the number of moving neighbors that Avilov and Iordansky consider around the exchanging particles is too small to obtain a realistic comparison of the various exchange frequencies. In particular, for triple exchange they only consider one moving neighbor (atom C in Fig. 10); if we follow the same assumption in our calculation we obtain $S_3=12.08$, instead of $S_3=9.27$ with $N=16$ moving atoms; this represents an overestimate of 30% of the exponent in the exponential. Their calculation of K_P is more reliable because they consider eight moving atoms; consequently, they dramatically disfavor three-particle exchange with respect to four-particle exchange.

It is also interesting to note that in our high-density calculation the lengths of the exchange paths are practically the same (of the order of $1.1a$) for planar four-, three-, and two-particle exchange. This property is also essentially related to the lattice geometry and it will certainly remain true at physical densities for bcc ^{3}He.

If planar four-, three-, and two-particle exchanges have a comparable tunneling barrier height V, and the same path lengths L, we expect that they vary according to practically the same law in terms of the molar volume. We can thus understand the recent experimental results on the variation of the thermodynamic quantities in bcc solid ^{3}He.[9–12] This last point will be discussed in more detail in the following section.

It is interesting to given an order of magnitude of the ratios between $K_P, J_t, J_{\rm NN}, \ldots$, at physical densities ($v \simeq 23 \sim 24$ cm^3/mol), assuming that the relative differences of the exponents S_P remain of the same order as in the high-density limit:

$$(S_{J_t}-S_{K_P})/S_{K_P} \simeq 10\%, \quad (S_{J_{\rm NN}}-S_{J_t})/S_{J_{\rm NN}} \simeq 12\% \ .$$

At $V \simeq 24.2$ cm^3/mol, K_P is of the order of 0.4 mK; the Debye temperature is 20 K.

The exponent S_{K_P} in the exponential ($K_P \sim \Theta_D e^{-S_{K_P}}$) is of the order of $\ln(5\times 10^4) \sim 11$. Hence, the ratio between K_P and J_t or between J_t and J_{NN} would be of the order of $e^{1.1-1.3} \simeq 3-4$. We have not taken into account the prefactors α_T which might differ by order 1 from one exchange constant to the other. In addition, we have not taken into account the symmetry factor (12) of J_{NN}.

Hence we conclude that the ratio between K_P and J_t would be of order of 3 to 4 and, due to the symmetry factor, J_{NN} might be of the same order as J_t or K_P. Only the Monte Carlo calculation suggested in Sec. III could determine the exact ratio between J_{NN} and J_t. If J_{NN} is of the same order as J_t, the experimental data could be interpreted with a three-parameter model. This model would lead to a better fit of the critical field between the *uudd* and *pf* phases (see Ref. 1, Sec. XI B).

V. EXCHANGE AT PHYSICAL DENSITIES IN SOLID ^{3}He

In the preceding sections we have determined the first terms of a high-density series expansion for the exchange frequencies. It is now important to discuss to what volume range this calculation applies. We will also present crude approximations for lower densities where an expansion in σ/a limited to the first terms is certainly unrealistic. We will discuss the variation of the exchange constants with the molar volume and compare the experimental results.

A. In what density range can we trust the WKB calculation for exchange in hcp ^{3}He? Comparison with the experimental data for hcp ^{3}He and for the two dimensional triangular lattice

Since, in the critical configuration, the distances a' between the exchanging particles are appreciably reduced ($a' \simeq 0.8a-0.9a$), the quasiclassical limit is certainly more appropriate for exchange calculations than for the determination of physical properties involving mainly the equilibrium configurations. The WKB calculation is certainly realistic at least up to $a \simeq \sigma/0.8 \simeq 3.2$ Å ($\sigma \simeq 2.556$ Å for helium).

To get a more precise idea of the applicability range of the quasiclassical approximation, it seemed interesting to us to investigate the variations of the energy, pressure, and compressibility in terms of the molar volume for the highest densities experimentally attained. In the classical limit, the energy of the solid reduces to the potential energy

$$V = \sum_{i<j} 4\epsilon \left| \frac{\sigma}{r_{ij}} \right|^{12}$$

(repulsive part of the Lennard-Jones potential). The energy per atom is

$$\mathscr{E} = \frac{n}{2} 4\epsilon \left[\frac{\sigma}{a} \right]^{12}$$

($n=12$ is the number of first neighbors and a is their distance).

In terms of the atomic volume $v = a^3/\sqrt{2}$ (we take the hcp lattice), we have

$$\mathscr{E} = 6\epsilon(\sigma^3/v)^4 .$$

The pressure is

$$P = \frac{-\partial \mathscr{E}}{\partial v} = \frac{24\epsilon}{\sigma^3} \left[\frac{v}{\sigma^3} \right]^{-5} , \tag{5.1}$$

and the compressibility is

$$K = -\frac{1}{v}\frac{\partial v}{\partial P} = \frac{\sigma^3}{120} \left[\frac{v}{\sigma^3} \right]^{5} . \tag{5.2}$$

Both pressure and inverse compressibility vary in v^{-5}. Our first idea was to plot $P(v)$ and $K^{-1}(v)$ in logarithmic coordinates and find the density at which a deviation from the v^{-5} law is observed. We took the data from Refs. 28–30 and were surprised to obtain a linear dependence of $\ln P$ and $\ln K$ in terms of $\ln v$ with slopes practically equal to -5 and $+5$ in a wide volume range proceeding from the highest measured densities in hcp ^{3}He to the lowest densities of the bcc phase [see Fig. 13(a)].

Moreover, relations (5.1) and (5.2) can be fitted with $\epsilon = 10.22$ K and $\sigma = \sigma^* \simeq 2.65$ Å, the latter a value which is only 3.5% higher than the usual Lennard-Jones diameter, $\sigma \simeq 2.56$ Å. (Similar results are found in hcp ^{4}He [see Fig. 13(b)]; however, a deviation with respect to the v^5 law is observed at $v \gtrsim 17$ cm^3/mol.) Such power laws have been noticed previously in the literature for the elastic constants C_{ij} which vary in v^{-5} (Ref. 31) and the Debye temperature Θ_D varying as $v^{-7/3}$ (see Fig. 14, p. 646 of Ref. 32). However, to our knowledge, this universal variation law has received, up to now, no theoretical interpretation. This might partly be the result of an accidental cancellation between the kinetic energy and the attractive part of the Lennard-Jones potential, both of which are neglected in the high-density limit. This last remark is based on the results given in Table III. We compare, for hcp ^{4}He, the kinetic energy of a hard-sphere solid calculated by Monte Carlo processes[33] to the attractive part of the Lennard-Jones potential [the hard-core diameter a_{HC} is chosen as the scattering length corresponding to the Lennard-Jones potential $a_{HC} = 0.8368\sigma$ (Ref. 33)]. In a wide volume range from $v \simeq 11.8$ to 24.14 cm^3/mol, the kinetic energy and the attractive part of the Lennard-Jones potential cancel almost exactly (with an accuracy better than 2.5%).

The interaction energy $\mathscr{E}(\vec{r})$ of one atom at position $\vec{r} = (x,y,z)$ with all its neighbors, supposedly fixed at the equilibrium positions (lattice sites), is a very flat function $\mathscr{E}(x,y,z)$ in a wide domain around $\vec{r} = \vec{0}$, with a weak maximum at the central position $\vec{r} = \vec{0}$. In this wide region, $\mathscr{E}(\vec{r})$ is practically constant and equal to the value $\mathscr{E}_0$ of the interaction potential at $\vec{r} = \vec{0}$. At the edges of this domain, $\mathscr{E}(\vec{r})$ is dominated by the hard-core repulsion and it rises very abruptly. As a consequence it makes sense to approximate the energy, *measured from* $\mathscr{E}_0$, by the energy of the hard-core solid, $\mathscr{E}_{HC}$,

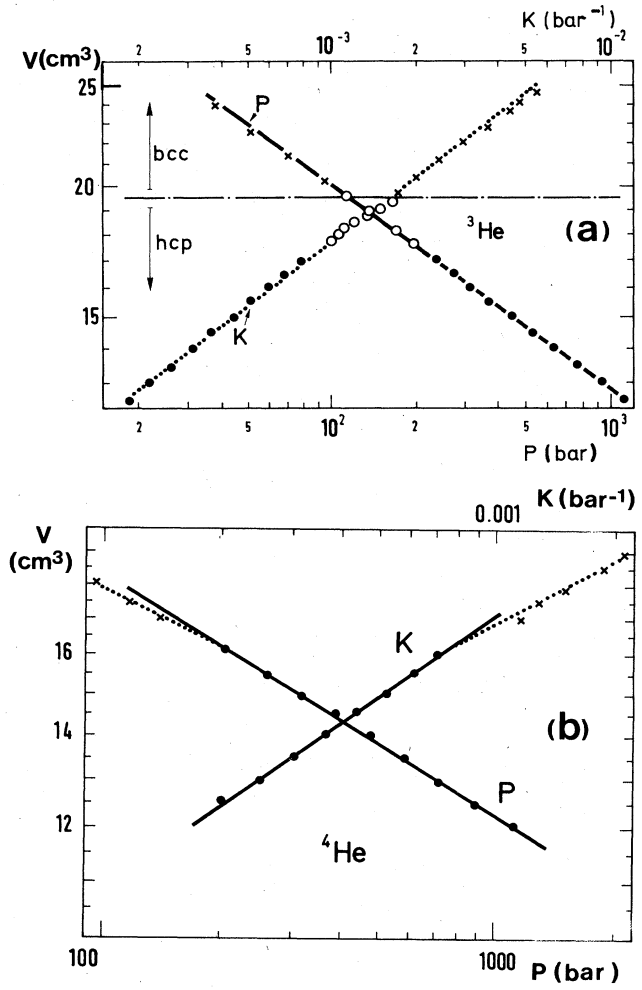

FIG. 13. Variation of the pressure and compressibility of solid He in terms of the molar volume. (a) ^{3}He: Experimental points are from Dugdale and Franck (Ref. 28) (●) for hcp ^{3}He at high densities, and from Straty and Adams (Ref. 30) (○, hcp phase; ×, bcc phase). (b) ^{4}He: Experimental points are from Dugdale and Franck (Ref. 28) (●), and from Edward and Pandorf (Ref. 29) (×).

TABLE III. Comparison of the kinetic and potential energy in hcp ^{3}He. The kinetic energy $\mathscr{E}_{HC}$ estimated as the energy for a hard-sphere solid with hard-core diameter 0.8368σ (third column) cancels almost exactly with the attractive part of the Lennard-Jones potential (fourth column). The sum of $\mathscr{E}_{HC}$ and the Lennard-Jones potential reduces practically to the repulsive part of the Lennard-Jones potential varying in $(\sigma/a)^{12}$ (fifth column) ($\epsilon=-10.22$ K and $\sigma=2.556$ Å are the parameters of the Lennard-Jones potential; $n=12$ is the number of first neighbors).

V (cm^3)	a/σ	$\mathscr{E}_{HC}$ (K)	$-\frac{n}{2}4\epsilon\left[\frac{\sigma}{a}\right]^6$	$\frac{n}{2}4\epsilon\left[\frac{\sigma}{a}\right]^{12}$
21.81	1.453	26.5	−26.0	2.8
19.64	1.403	32.15	−32.15	4.2
14.74	1.275	55.7	−57.1	13.3
11.77	1.183	90.3	−89.3	32.5

$$\mathscr{E}=\mathscr{E}_0+\mathscr{E}_{HC}\,. \tag{5.3}$$

(This approximation was first suggested by London.[34])

Applying (5.3) and taking into account the fortuitous cancellation between the hard-core kinetic energy and the attractive part of the Lennard-Jones potential, we obtain

$$\mathscr{E}\simeq\mathscr{E}^{12}=\frac{n}{2}4\epsilon\left[\frac{\sigma}{a}\right]^{12}.$$

This justifies the v^{-5} law for the pressure variations beyond the quasiclassical limit. For ^{3}He we obtain a partial but not exact cancellation.

This discussion on the ground-state energy of solid He leads us to the following conclusion about exchange: Owing to this fortuitous cancellation, the next-order terms in g^0 and $g^{1/5}$ in the WKB expansion, which take, respectively, into account the kinetic energy and the attractive part of the Lennard-Jones potential [see Sec. IV A 1 and relations (4.7) and (4.8)], might also partly cancel. In this case, our calculation could be reasonably extrapolated at lower densities.

Let us apply this calculation to exchange in the hcp lattice and compare our results to the experimental results. As shown in Sec. IV, triple exchange J_T (in the basal plane) and triple exchange J_T' (out of the basal plane) are dominant. Using (4.21), we write

$$J_T=\alpha_\perp 4\sqrt{2}\frac{\hbar^2}{2m(La)^2}\left[\frac{(V_M)^{1/2}L}{g}\right]^{3/2}\exp\left[-\frac{1}{g}S_3\right], \tag{5.4}$$

with

$$g=\frac{\hbar}{(8m\sigma^2\epsilon)^{1/2}}\left[\frac{a}{\sigma}\right]^5,\quad S_3=\frac{4}{\pi}(V_M)^{1/2}L\,.$$

From Table II we have $(V_M)^{1/2}L=7.33$ and $L=1.00$ for J_T, and $(V_M)^{1/2}L=7.75$ and $L=1.00$ for J_T'. We take for the Lennard-Jones parameter σ the effective value $\sigma=\sigma^*=2.65$ Å, which fits, respectively, the v^{-5} and v^5 laws for the experimental pressure and compressibility curves [see relations (5.1) and (5.2)].

A rough evaluation of the prefactor $\alpha_\perp$ has been proposed in Sec. IV [relations (4.16) and (4.17)]. An order of magnitude of $\alpha_\perp$ for J_T is estimated from Fig. 7 in the following way.

In the critical exchange configuration the atoms for which the available space is appreciably reduced are the three exchanging atoms (atoms of type A on the figure) and their three nearest neighbors (type-B atoms). For the three exchanging atoms the available space is reduced only in one direction (that of the closest atoms in the basal plane). The distance to the next neighbors is about $0.85a$.

For the three type-B atoms the free space is mainly reduced in one direction, that of the closest exchanging atoms (the distance is $\sim 0.85a$). The available place is more slightly reduced in the direction perpendicular to the basal plane (the distance to the closest atoms being $\sim 0.92a$).

From relations (4.16) and (4.17), we estimate that

$$\alpha_\perp\simeq(0.85^{14})^{3/4}(0.85^{14})^{3/4}(0.92^{14})^{3/4}\simeq 10^{-2}\,. \tag{5.5}$$

Assuming the same order of magnitude of $\alpha'_\perp$ for J'_T, we obtain

$$J_T/k_B \simeq 18.7 \left[\frac{\sigma^*}{a}\right]^{19/2} \exp\left[-55.8\left[\frac{\sigma^*}{a}\right]^5\right] \text{K} ,$$
$$J'_T/k_B \simeq 19.7 \left[\frac{\sigma^*}{a}\right]^{19/2} \exp\left[-59.0\left[\frac{\sigma^*}{a}\right]^5\right] \text{K} . \quad (5.6)$$

In Fig. 14 we compare effective mean values of the pair interaction J_{eff} deduced from nuclear-magnetic-resonance (NMR) measurement[35] to the theoretical curve

$$J_{\text{eff}} = \frac{\Theta}{6} = \tfrac{1}{2}(J_T + 6J'_T)$$

[see relation (4.40)] obtained from (5.6). The agreement is good. [Note that we are essentially interested in comparing the slopes of these curves ($\partial \ln\Theta/\partial \ln a$) because the exponents S_3 and S'_3 of the exponentials have been calculated accurately. Only the orders of magnitude of α_T and α'_T have been estimated. In addition, the NMR does not measure Θ, but instead further complicates functions of J_T and J'_T.]

Let us now consider the two-dimensional triangular lattice. Triple exchange is given by relation (5.4) with $S_3 = 8.65$ and $L = 1.07$ (see Sec. IV C 1 b). The prefactor is estimated in the same way as for the exchange in the basal plane of the hcp lattice.

From Fig. 1(a) the distances between the exchanging particles and their nearest neighbors are reduced to $\sim 0.87a$. The free space is reduced essentially in one dimension for the three exchanging particles and their closest neighbors. Hence,

$$\alpha_\perp \simeq (0.87^{14})^{6/4} \simeq 5 \times 10^{-2} .$$

We deduce

$$J_T/k_B \simeq 73 \left[\frac{\sigma^*}{a}\right]^{19/2} \exp\left[-51.7\left[\frac{\sigma^*}{a}\right]^5\right] \text{K}$$

(we again choose $\sigma = \sigma^* = 2.65$ Å).

The curve obtained is compared in Fig. 15 to the experimental results of Richards.[36] We again emphasize that we must essentially compare the slopes $\partial \ln J_t/\partial a$ of the theoretical and experimental curves because (i), $\alpha_\perp$ is only roughly estimated, and (ii) the experimental values are deduced from relaxation-time measurements, and the exact relations between these times and J_T are not known. The agreement is satisfying.

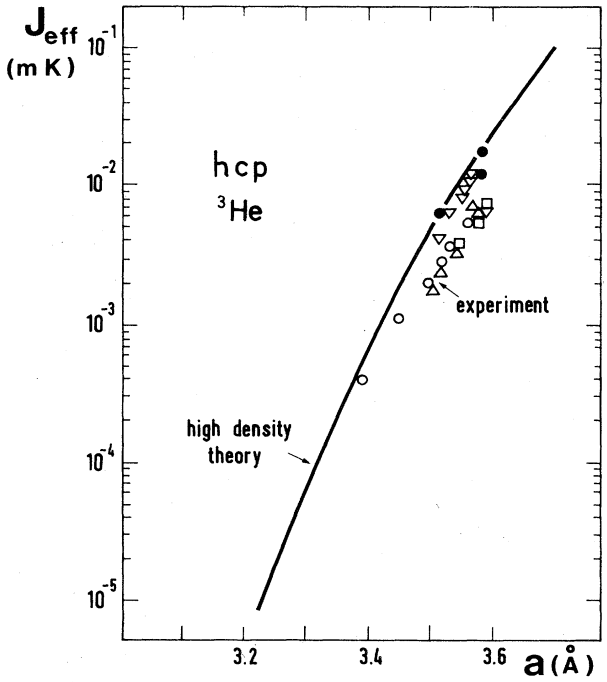

FIG. 14. Comparison of the experimental values of exchange frequencies in hcp solid ^{3}He with the extrapolated high-density theory. The experimental points are effective values of pair spin interaction J_{eff} deduced from NMR measurements and taken from Fig. 31 of the review paper by Guyer *et al.* (Ref. 35). We compare these values to the theoretical curve, $J_{\text{eff}}(a) = (\Theta/6)(a) = \frac{1}{2}(J_T + 6J'_T)$. We recall that the prefactors α_T and α'_T in J_T and J'_T are only roughly estimated and that we must essentially compare the slope $\partial \ln J_{\text{eff}}/\partial \ln a$ to that deduced from the experimental points.

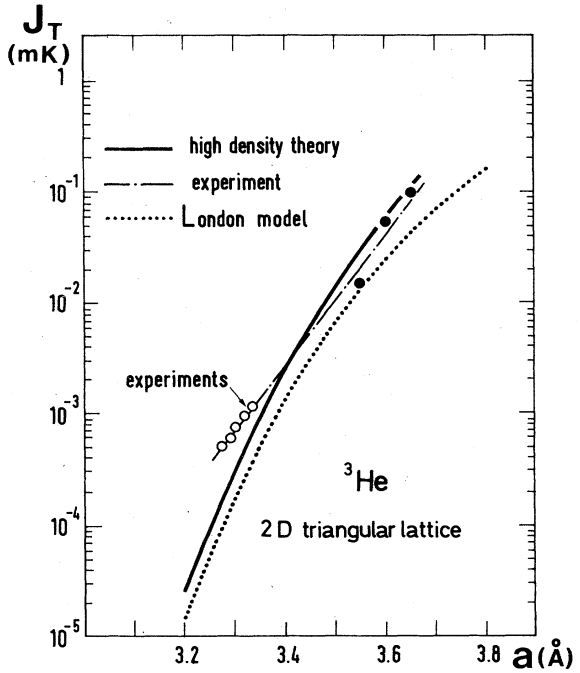

FIG. 15. Comparison of the experimental values of exchange in two dimensions, deduced from nuclear magnetic resonance, to the theoretical predictions. Both sets of points (○ and ●) are from Richards (Ref. 36). They are deduced from different relaxation times. They represent J_T within an unknown multiplicative factor of order 1. The solid curve represents the extrapolation to intermediate densities of our high-density series expansion limited to the first terms. The dotted line represents the crude approximation described in Sec. B using the "London model." We must essentially compare the slopes of these curves (the preexponential factors have been crudely estimated).

B. Crude approximation for low densities

At physical densities for bcc ^{3}He ($20 \lesssim v \lesssim 24.2$ cm^3/mol the application of a high-density series expansion limited to the first terms is suspect. For these low densities, crude approximations for exchange calculations have been proposed earlier.[1-4]

The leading idea of all these approximations is to reduce the $3N$ variable problem to a one-dimensional Schrödinger equation,

$$-\frac{\hbar^2}{2m}\Delta\psi(t)+\tilde{V}(t)\psi(t)=E\psi(t) , \tag{5.7}$$

where t is the one-dimensional variable representing the curvilinear coordinate along a path $\mathscr{L}(t)$ joining the centers of the two cavities Ω_I and Ω_P. $\tilde{V}(t)$ is an effective potential which represents essentially the energy in the $(3N-1)$-dimensional space orthogonal to the tangent at t to the path $\mathscr{L}(t)$.

Various approximations have been suggested to estimate $\tilde{V}(t)$. The crudest but simplest was proposed by Delrieu and Sullivan in Ref. 2. Using a crude elastic model of deformation around the exchanging particles, they estimated the effective potential barrier from the experimental data on pressure P and compressibility K. As both P and K^{-1} vary in v^{-5} (see Sec. V A), this model leads to a variation of $\tilde{V}$ in $(\sigma^*/a)^{12}$ and gives exchange constants in $\exp[-A_p(\sigma^*/a)^5]$; this is the same functional form as that obtained in the high-density limit. This model correctly fits the experimental data for both the hcp and bcc phases of solid ^{3}He (cf. Fig. 4 of Ref. 2). The optimization of the exchange path has not been treated completely in Ref. 2; however, it could be done in the same way as for the high-density limit [i.e., find the classical path $\mathscr{L}(t)$ for a particle moving under the action of an effective potential $\tilde{V}(r)$; see Refs. 1 and 37].

More recently, Avilov and Iordansky[8] proposed a model in which the experimental data on the elastic properties of bcc ^{3}He are also used to build up an effective interaction potential between He atoms. They apply the quasiclassical approximation to determine the exchange path. The use of the experimental elastic constants which vary according to a universal law [$P\sim(\sigma^3/v)^5$, $K\sim(v/\sigma^3)^5$, and $\Theta_D\sim(v/\sigma^3)^{-7/3}$] also leads to an effective potential in $(\sigma/a)^2$ and a functional form in $\exp[-A_p(\sigma/a)^5]$ for the exchange frequencies. The main criticism that we address to their model is the following: The number of moving particles that they consider is too small to give a realistic estimation of the classical path and of the action S along the path (cf. Sec. IV E 3). Just like the calculation presented in this paper, this model applies essentially in the high-density limit.

In earlier papers Delrieu *et al.*[6] proposed an estimation of the effective potential $\tilde{V}(t)$ using the simple London model.[34] Again, in Ref. 6 the path has not been optimized completely. Here, we would like to improve this model with a simple but realistic optimization of the exchange path and compare the experimental results.

Let us first review the approximation of the ground-state energy of He proposed by London. The energy of He is estimated as the sum of the kinetic energy $\mathscr{E}_{\rm HC}$ of a hard-sphere gas and of the Lennard-Jones interaction potential $\mathscr{E}_0$ for the equilibrium position. [This approximation has been justified in Sec. V A, see Eq. (5.3).] The kinetic energy per particle is estimated as the energy of a point mass in a sphere of radius δ, δ being the maximum possible excursion of the particle when its neighbors are fixed at the lattice sites. In three dimensions,

$$\mathscr{E}_L^3=\pi^2/3\delta^2 .$$

It is remarkable to note that for hcp He this crude estimation gives good results compared to the exact Monte Carlo calculation.[33,37]

To justify this crude estimation it is interesting to consider the results of exactly soluble models which are not so far from our problem (at least for the calculation of the ground-state energy).

(i) The problem of a one-dimensional hard-sphere fermion gas can be solved exactly. The ground-state energy is

$$\mathscr{E}_{\rm HC}^l=\pi^2/3\delta^2 .$$

(Note that the London approximation gives $\pi^2/4\delta^2$.)

(ii) In three dimensions the energy for independent rows of hard-cube fermions submitted to the conditions [for all i,j,k (i,j,k label the lattice sites)],

$$(x_{i+1,j,k}-x_{i,j,k})<\sigma ,$$

$$(y_{i,j+1,k}-y_{i,j,k})<\sigma ,$$

$$(z_{i,j,k+1}-z_{i,j,k})<\sigma$$

is deduced easily by

$$\mathscr{E}_{\rm HC}^3=3[\pi/(3\delta^2)]=\pi^2/\delta^2 ,$$

where $\delta=a-\sigma$ (a represents the distance between first neighbors).

This value is certainly a good approximation for the ground-state energy of a simple-cubic hard-cube solid. We also expect this approximation to be realistic for a compact hard-sphere lattice. We note that in three dimensions the London value $\mathscr{E}_L^3$ is fortuitously identical to this approximation $\mathscr{E}_{\rm HC}^3$. In two dimensions, the London value ($\mathscr{E}_L^2=0.59\pi^2/\delta^2$) is lower with respect to $\mathscr{E}_{\rm HC}^2=2\pi^2/3\delta^2$; in one dimension $\mathscr{E}_L^1=\frac{3}{4}\mathscr{E}_{\rm HC}^l$. In the following we shall take $\mathscr{E}_{\rm HC}$ (rather than $\mathscr{E}_L$) as an estimation for the hard-core solid energy. We shall restrict our calculation to the two-dimensional lattice.

We apply the elementary approximation described in Sec. IV B 1 to the effective potential $\tilde{V}(t)$ in Eq. (5.7). Thus, we have to estimate the barrier height $\tilde{V}_M=\tilde{V}_\Sigma-\tilde{V}_0$. $\tilde{V}_0=\mathscr{E}_0+\mathscr{E}_{\rm HC}^2$ is taken as the ground-state energy calculated by the method described above. $\tilde{V}_\Sigma$ represents the energy in the critical exchange configuration. The kinetic energy in the critical exchange configuration is estimated through the following process: For each particle we take

$$\mathscr{E}_K^i=\frac{1}{n}\sum_{j=1}^{n}\frac{2}{3}\frac{\pi^2}{\delta_{ij}^2} , \quad \delta_{ij}=|r_{ij}|-\sigma .$$

The sum is extended to the n nearest neighbors (by nearest

neighbors in the critical exchange we mean particles whose distance is smaller than a fixed value $R_0 \gtrsim a$). We write

$$\tilde{V}_\Sigma = \sum_{i=1}^{n} \mathscr{E}_K^i + \sum_{\substack{i<j \\ i,j=1}}^{n} V_{\mathrm{LJ}}^{ij} ,$$

the second term representing the Lennard-Jones interaction in the critical exchange configuration. According to the method described in Sec. IV B 1, the critical exchange configuration is obtained by minimizing the action $S_P = -(4/\pi)(V_M)^{1/2}L$. We have essentially used this method to determine the variations of triple exchange J_T with the molar volume in the triangular lattice.

We take as hard-core diameter the scattering length for particles interacting via the $(\sigma/r)^{12}$ potential, [$\sigma_{\mathrm{HC}} = 0.8368\sigma = 2.139$ Å (see Ref. 33)]. On Fig. 16 we show the particles positions in the critical exchange configuration and give further details on the way we estimate the kinetic energy. Table IV gives the values of L^2 and $S_3' = \sqrt{V}\,L$ for various interatomic spacing. In Fig. 15 we compare the curve

$$J_T \simeq 4\sqrt{2}\frac{\hbar^2}{2m\,(La)^2}(S_3')^{3/2}\exp\left[-\frac{4}{\pi}S_3'\right]$$

thus obtained with the high-density limit and with the NMR measurements of Richards.[36] The agreement with the experimental results and with the extrapolation of the high-density limit is satisfying. We are content to be interested in the exponent S_3' and its variations with molar volume (i.e., to the slope $\partial \ln J_T/\partial a$; our approximation is too rough to give accurate values of J_T).

C. Variations of the exchange constants with molar volume in bcc ^{3}He

The experimental data on bcc ^{3}He cannot be interpreted with only one dominant exchange process (see Ref. 1), we need at least planar four-particle exchange K_P and triple exchange J_t (perhaps pair exchange J_{NN} also). The recent experiments on the variation of some thermodynamic quantities with molar volume can be understood only if

TABLE IV. Path length L, action (exponent) S_3', and triple-exchange frequency J_T versus interatomic distance a within the crude "London approximation."

a (Å)	L^2 (units of a^2)	S_3'	J_T (mK)
3.8	1.29	10.31	1.61×10^{-1}
3.7	1.28	11.11	6.90×10^{-2}
3.6	1.27	12.14	2.26×10^{-2}
3.5	1.26	13.25	6.69×10^{-3}
3.4	1.25	14.65	1.40×10^{-3}
3.3	1.25	16.56	1.58×10^{-4}
3.2	1.245	18.69	1.33×10^{-5}

$$J_T = 4\sqrt{2}\frac{\hbar^2}{2ma^2L^2}(S_3')^{3/2}\exp\left[-\frac{4}{\pi}S_3'\right]$$

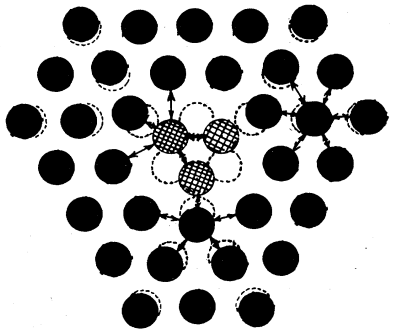

FIG. 16. "London" approximation. We have represented the particle positions in the critical configuration for $a = 1.59\sigma_{\mathrm{HC}}$ (the scale for the hard-core diameter is respected on the figure). The kinetic energy per particle is estimated as the mean value $(1/n)\sum_i \frac{2}{3}(\pi^2/\delta_i^2)$, where the δ_i are the distances shown by the arrows; n is the number of neighbors which are taken into account. For the exchanging particles (cross-hatched circles) this sum reduces practically to $\frac{3}{5}\times\frac{2}{3}(\pi^2/\delta^2)$ where δ is the common distance to the three closest particles; we think that this estimate is reasonable because, due to the geometry of the figure, the localization of these particles is practically one dimensional (the free space between particles is appreciably reduced only in one direction); in strictly one dimension we would obtain $\frac{1}{3}(\pi^2/\delta^2)$.

all exchange frequencies vary according to similar laws in terms of the molar volume[8–10,38] i.e.,

$$\frac{\partial \ln J_t}{\partial v} \simeq \frac{\partial \ln K_P}{\partial v} \simeq \frac{\partial \ln J_{\mathrm{NN}}}{\partial v} .$$

We are now able to give a theoretical interpretation of this experimental observation.

We have seen that in the high-density limit, planar four-particle exchange, triple exchange, and pair exchange lead to close values for the action $S_{K_P} \lesssim S_{J_T} \lesssim S_{J_{\mathrm{NN}}}$, and also to practically the same length for the exchange path $L \simeq 1.1$. As emphasized in Sec. IV C, we believe that this property depends essentially on the lattice geometry and not on the exact shape of the effective potential barrier. We expect that this property remains true at all densities and leads to similar variations of J_t, K_P, and J_{NN} with the molar volume.

The models based on the universal v^{-5} variation law of the experimental elastic constants suggest that the functional form

$$J_P \sim \Theta_D \exp[-f(a)], \quad f(a) = S_P'(\sigma/a)^5$$

obtained in the high-density limit extrapolates at low densities, up to the bcc phase near melting. These models are crude and their validity is questionable. However, we must emphasize that this functional form gives remarkable agreement for the last experimental results[7–12] concerning the Grüneisen constant $\partial \ln J_P/\partial \ln V$. We have

$$\frac{\partial \ln J_P}{\partial \ln V} = \frac{1}{3}\frac{\partial \ln J_P}{\partial \ln a} \simeq \frac{5}{3}f(a) \simeq \frac{5}{3}\ln\left[\frac{\Theta_D}{J_P}\right] .$$

We have seen that the exponents $f(v)$ for K_P and J_t only differ by about 10%. At 24 cm^3/mol, $f(a) \simeq \ln(\Theta_D/J) \simeq 11$. Hence, within 10%,

$$\frac{\partial \ln K_P}{\partial \ln v} \simeq \frac{\partial \ln J_t}{\partial \ln v} \simeq \frac{5}{3} \times 11 \simeq 18 .$$

A more careful analysis of the recent experimental results is given in Ref. 12.

VI. CONCLUSION

We have determined the first terms of a high-density series expansion for the exchange frequencies in solid ^{3}He and the lowest-order term of a low-density series expansion for exchange in the two-dimensional Wigner solid of electrons. The hierarchy between various multiple-exchange processes depends essentially on the geometry of the lattice. In the two-dimensional triangular lattice, three-particle exchange dominates. The same hierarchy is also found with the $(\sigma/r)^{12}$ potential (^{3}He atoms adsorbed on a substrate for high coverage) and with the Coulomb potential (Wigner solid of electrons at low densities). Triple exchange also dominates in the hcp lattice. The theoretical high-density limit, in the bcc phase, gives the following hierarchy: K_P (planar four-particle exchange) $> J_t$ (triple exchange) $\gtrsim J_{NN}$ (pair exchange) $> S_{IX}$ (six-particle exchange) $> K_F$ (folded four-particle exchange). We think this hierarchy is essentially related to the geometry and is unchanged at lower densities. This hierarchy is precisely that which was inferred from the experimental data.[1] Moreover, we find that the lengths L of the exchange paths are practically the same for planar four-particle exchange K_P, triple exchange J_t, and pair exchange $J_{\rm NN}$, and that the actions

$$S_P \sim (V_M)^{1/2} L$$

only differ by about 10%. We have shown that these properties are essentially related to the lattice geometry and do not depend on the detailed structure of the potential. Hence, we expect that these results remain approximately valid at lower densities. At the densities of the bcc phase, S_P is of the order of 10 and relative differences of 10% in the S_P's lead to factors of the order of $\exp(1) \simeq 3$ between various exchange frequencies (K_P, J_T, and $J_{\rm NN}$). We clearly understand why several exchange processes (K_F, J_t, and perhaps $J_{\rm NN}$) play an essential role in the experimental magnetic properties of solid bcc ^{3}He.

As the path lengths L are practically the same for K_P, J_t, and $J_{\rm NN}$, and the potential barriers are comparable, we also expect that these three frequencies vary according to very similar law in terms of the molar volume. This removes the last objections raised against the multiple-exchange model.[9-12]

As three-particle exchange leads to ferromagnetism we predict a positive Curie-Weiss constant Θ in hcp ^{3}He and in a monolayer of a ^{3}He atom adsorbed on a substrate. We encourage experimentalists to measure Θ in these systems; this could provide an excellent test of the theory, especially at high density.

Further theoretical calculations at physical densities for bcc ^{3}He could be performed from a path-integral formulation using Monte Carlo integration. In particular, the ratios between various exchange constants could be calculated exactly. We think this method is worth investigating in the near future.

ACKNOWLEDGMENTS

We are indebted to J. M. Delrieu and N. Sullivan for stimulation and illuminating suggestions. We thank Professor D. Nozières for helpful criticism and judicious remarks. We thank B. Castaing, H. Godfrin, and J. H. Hetherington for encouraging discussions.

APPENDIX: LARGER-ORDER CYCLIC ν PARTICLE EXCHANGE (TWO DIMENSIONS)

Here, we give a rough estimate of the decrease of the exchange frequency J_ν with increasing ν for symmetric cyclic exchange with a large number ν of particles in the two-dimensional case.

Figure 1(e) in Sec. IV shows the critical configuration for a block rotation of 12 particles. It is obvious that such a block rotation leads to a barrier height V_M increasing roughly proportionally to the number n of exchanging particles. For large ν it will be energetically more favorable to create a pair vacancy interstitial and exchange will occur through the separation of this pair vacancy interstitial. In order to give a rough order of magnitude of the exchange frequency corresponding to this process, we consider the following schematic model.

We consider ν particles on a circle (Fig. 17); we represent the effect of the surrounding particles by a sinusoidal potential

$$V = \tfrac{1}{2} v_M \sin(\pi t/a) , \tag{A1}$$

where t is the arc length on the circle. The value of v_M is estimated through Fig. 1(e). In the critical configuration represented on this figure, the barrier height is $V_M = 65.7$ (in reduced units). Part of this barrier comes from the reduction in the distance between the exchanging particles,

$$\Delta V_1 = 12[(0.936)^{-12} - 1] = 14.5 .$$

The remainder, $V_M - \Delta V_1 = 51.2$, is due to the compression of surrounding particles. We deduce $v_M \simeq 51.2/12 = 4.3$. The particles and the potential are represented

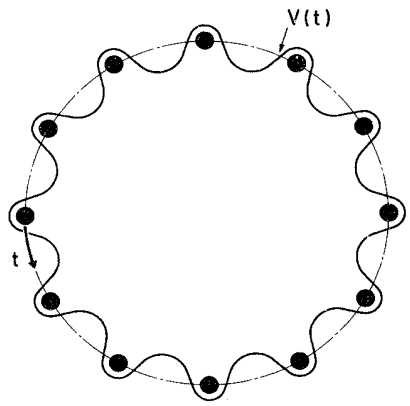

FIG. 17. Effective potential $V(t) \simeq (v_M/2)\sin(\pi/a)t$, due to the neighboring atoms.

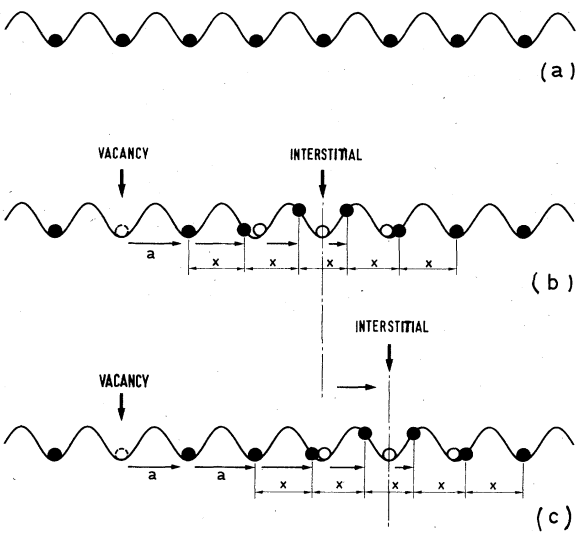

FIG. 18. Creation and separation of a pair vacancy interstitial. The interstitial is schematized by a uniform compression of the chain along a distance νx with $x=a(\nu-1)/\nu$. A translation of the interstitial does not change the energy.

on a linear axis t with periodic boundary conditions in Fig. 18(a).

1. Energy for the formation of a pair vacancy interstitial

We take the following crude model for the pair vacancy interstitial. We assume that one particle is displaced of one interatomic distance a and that the chain is uniformly compressed over a distance $(n-1)a$; the number n of particles involved in this process is optimized to give the lowest-energy barrier.

There are n pairs of atoms whose distance is reduced at the value $x=(n-1)a/n$. The potential increase due to this uniform compression is

$$\Delta V_1=n\{[n/(n-1)]^{12}-1\} .$$

If n is large, the potential increase due to the compression of the neighboring atoms [sinusoidal potential of relation (A1)] is practically

$$n\int_{-1/2}^{+1/2}\frac{v_M}{2}\left[1-\sin\frac{\pi}{a}t\right]=nv_M/2 .$$

The total barrier height is

$$V_M^v=n\{[n/(n-1)]^{12}+v_M/2-1\} , \tag{A2}$$

with $v_M=4.3$; the minimum of V_M^v is obtained with $n\simeq 10$ particles with a barrier height of $V_M^v\simeq 47$.

The total length in the configuration space corresponding to the particle displacements is

$$L^v=a\left[\sum_{i=0}^{n-1}\left[\frac{n-i}{n}\right]^2\right]^{1/2}\simeq 1.96a . \tag{A3}$$

2. Exchange via the separation of the pair vacancy interstitial

Suppose that the number ν of exchanging particles is large compared to 10 ($\nu\simeq 20-30$). Once the pair vacancy interstitial has been created, we can translate the interstitial (increase the distance between the vacancy and the interstitial) without appreciable energy change. The exchange will occur through this translation. The barrier will be practically flat. The configuration X_M on the median hyperplane Σ is obtained when the position of the vacancy and the interstitial are opposite on the exchange circle. The exchange barrier is represented in Fig. 19. We approximate the first part by a sinusoid. The action is

$$S_\nu=\frac{4}{\pi}(V_M^v)^{1/2}\left\{L^v+\frac{\pi}{2}\left[\left[(L^v)^2+\frac{\nu-n}{2}\right]^{1/2}-L^v\right]\right\} , \tag{A4}$$

with the numerical value given in subsection 1 of this Appendix we find

$$S_\nu\simeq 13.7\left[\left[\frac{\nu}{2}-1.16\right]^{1/2}-0.71\right] . \tag{A5}$$

3. Behavior of the exchange frequency J_ν with S_ν for large order symmetric cyclic exchange ($\nu\gtrsim 6$)

The relation (A5) shows that for very large ν ($\nu\gg 10$) the exchange frequency J_ν decreases as

$$J_\nu\simeq\exp(-9.7\sqrt{\nu}) . \tag{A6}$$

On the other hand, for $6\lesssim\nu\lesssim 12$ we have seen that a block rotation of the particles is more favorable than exchange via the creation of a pair vacancy interstitial [see Figs. 1(c) and 1(e)].

For a block rotation [see the numerical results of Figs. 1(c) and 1(e)], the potential barrier is roughly proportional

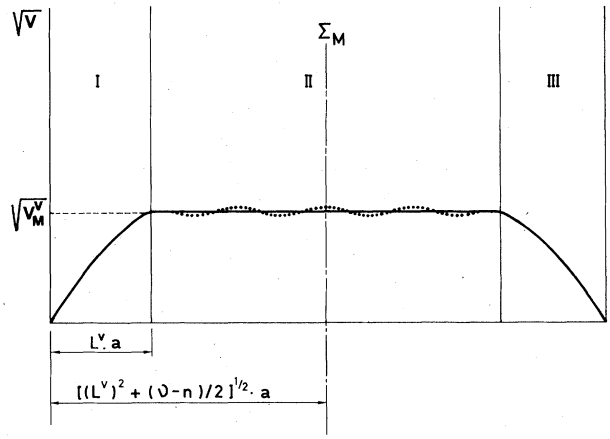

FIG. 19. Potential barrier for exchange through the creation of a pair vacancy interstitial. Part I corresponds to the creation of a pair vacancy interstitial. II is the interstitial moving apart; the intersection with Σ_M corresponds to opposite positions on the circle for the vacancy and the interstitial. III corresponds to the destruction of the pair vacancy interstitial.

to the number of exchanging particles,

$$V_M \simeq 5.5\nu ,$$

and the total displacement L in the configuration space is proportional to $\sqrt{\nu}$,

$$L^2 \simeq \nu a^2/4 ,$$

and hence

$$J_\nu \sim \exp(-1.5\nu) . \quad \text{(A7)}$$

It is important to estimate the number ν for which the change of regime occurs (i.e., the critical number ν for which exchange through the creation of a pair vacancy interstitial becomes more favorable). With the crude model described in subsection 1 (uniform compression), the potential barrier for a pair vacancy interstitial involving the uniform compression of ν particles is [relation (A2)]

$$V_M^v = \nu\{[\nu/(\nu-1)]^{12} + v_M/2 - 1\} .$$

The half-length of the corresponding exchange path is

$$L^v = a\left[\sum_{i=0}^{\nu-1}\left[\frac{\nu-i}{n}\right]^2\right]^{1/2} .$$

The action is

$$S_\nu^v = \frac{4}{\pi}(V_M^v)^{1/2} L^v .$$

The critical value of ν for which S_ν^v becomes smaller than 1.5ν [cf. relation (A7)] is

$$\nu_c \simeq 14 \text{ particles} .$$

Hence, for $6 \lesssim \nu \lesssim 14$ particles the exchange frequency decreases rapidly, as $\exp(-1.5\nu)$; for $\nu \gg 14$ the decrease will be slower [in $\exp(-9.7\sqrt{\nu})$ for $\nu \gtrsim 30$].

This estimation of ν_c is rough because our model is very crude. We have assumed a uniform compression, whereas the actual displacements are much more intricate. However, our complete minimization of $\sqrt{V}\,L$ on the exchange surface Σ_M (Sec. IV) for 12 particles leads to a block rotation (although the creation of a pair vacancy interstitial is allowed in the 60-variable minimization process). Hence, $\nu_c > 12$.

*Permanent address.

[1]M. Roger, J. H. Hetherington, and J. M. Delrieu, Rev. Mod. Phys. **55**, 1 (1983).

[2]J. M. Delrieu and N. S. Sullivan, Phys. Rev. B **23**, 3197 (1981).

[3]J. M. Delrieu and M. Roger, J. Phys. (Paris) Colloq. **39**, C6-123 (1978).

[4]A. K. Mc Mahan and R. A. Guyer, Phys. Rev. A **7**, 1105 (1973).

[5]A. K. Mc Mahan and J. W. Wilkins, Phys. Rev. Lett. **35**, 376 (1975).

[6]J. M. Delrieu, M. Roger, and J. H. Hetherington, J. Low Temp. Phys. **40**, 71 (1980).

[7]M. Roger, in *Proceedings of the International Conference on Magnetism (ICM '82)* (Kyoto, 1982) [J. Magn. Magn. Mater. **31-34**, 727 (1983)].

[8]V. V. Avilov and S. V. Iordansky, J. Low. Temp. Phys. **48**, 241 (1982).

[9]T. Mamiya, A. Sawada, H. Fukuyama, Y. Hiro, and Y. Masuda, Phys. Rev. Lett. **47**, 1304 (1981).

[10]T. Hata, S. Yamasaki, M. Taneda, T. Kodama, and T. Shigi, in *Proceedings of the International Conference on Magnetism (ICM '82) (Kyoto, 1982),* Ref. 7, p. 735.

[11]M. Devoret, A. S. Greenberg, D. Estève, N. S. Sullivan, and M. Chapellier, J. Low. Temp. Phys. **48**, 495 (1982); M. Bernier, Physica **114B**, 101 (1982).

[12]M. Roger, J. Phys. (Paris) Lett. **44**, L481 (1983).

[13]See for example, E. Landau and F. Lifschitz, *Quantum Mechanics* (Pergamon, New York, 1958).

[14]D. J. Thouless, Proc. Phys. Soc. London **86**, 893 (1965).

[15]R. P. Feynmann and A. Hibbs, *Quantum Mechanics and Path Integrals* (McGraw-Hill, New York, 1965).

[16]K. Binder, *Monte Carlo Methods* (Springer, Berlin, 1979).

[17]T. Banks, C. M. Bender, and T. T. Wu, Phys. Rev. D **8**, 3346 (1973); **8**, 3366 (1973).

[18]J. L. Gervais and B. Sakita, Phys. Rev. D **16**, 3507 (1977).

[19]B. R. Holstein and A. R. Swift, Am. J. Phys. **50**, 829 (1982).

[20]A. Abramowitz and I. A. Stegun, *Handbook of Mathematical Functions* (Dover, New York, 1972).

[21]A. Thomy and X. Duval, J. Chim, Phys. **67**, 286; **67**, 1101 (1970); C. Tiby, H. Wiechert, and H. J. Lauter, Surf. Sci. **119**, 21 (1982).

[22]See for example, J. M. Ziman, *The Principles of Solid State Physics* (Cambridge University Press, Cambridge, 1964).

[23]L. Bonsall and A. A. Maradudin, Phys. Rev. B **15**, 1959 (1977).

[24]C. Herring, in *Magnetism,* edited by G. T. Rado and H. Suhl (Academic, New York, 1966).

[25]C. C. Grimes and G. Adams, Phys. Rev. Lett. **42**, 795 (1979).

[26]K. Kajita and W. Sasaki, Surf. Sci. **113**, 419 (1982).

[27]For a review on 2D electron gases, see T. Ando, A. B. Fowler, and F. Stern, Rev. Mod. Phys. **54**, 437 (1982).

[28]J. S. Dugdale and J. P. Franck, Philos. Trans. R. Soc. London, Ser. A **257**, 1076 (1964).

[29]D. O. Edwards and R. C. Pandorf, Phys. Rev. **140**, A816 (1965).

[30]G. C. Straty and E. D. Adams, Phys. Rev. **169**, 232 (1968).

[31]R. Wanner, Phys. Rev. A **3**, 448 (1971).

[32]J. Wilks, *The Properties of Liquid and Solid Helium* (Clarendon, Oxford, 1967).

[33]M. H. Kalos, D. Levesque, and L. Verlet, Phys. Rev. A **9**, 2178 (1974).

[34]F. London, in *Superfluids* (Wiley, New York, 1954), Vol. II, Sec. 56, pp. 29–31.

[35]See the review paper by R. A. Guyer, R. C. Richardson, and L. I. Zane, Rev. Mod. Phys. **43**, 532 (1971).

[36]M. Richards, in *Phase Transitions in Surface Films,* edited by J. G. Dash and J. Ruvald (Plenum, New York, London).

[37]M. Roger, thesis, Université de Paris—Sud, 1980.

[38]K. Ishikawa *ICM'82 Conference, Kyoto, 1982,* poster session (unpublished).